

Pkd1 Regulates Lymphatic Vascular Morphogenesis during Development

Baptiste Coxam,¹ Amélie Sabine,² Neil I. Bower,¹ Kelly A. Smith,¹ Cathy Pichol-Thievend,¹ Renae Skoczylas,¹ Jonathan W. Astin,³ Emmanuelle Frampton,¹ Muriel Jaquet,² Philip S. Crosier,³ Robert G. Parton,¹ Natasha L. Harvey,⁴ Tatiana V. Petrova,² Stefan Schulte-Merker,⁵ Mathias Francois,^{1,6} and Benjamin M. Hogan^{1,6,*}

¹Institute for Molecular Bioscience, The University of Queensland, Brisbane, QLD 4072, Australia

²Department of Oncology, University Hospital of Lausanne, and Department of Biochemistry, University of Lausanne, 1066 Epalinges, Switzerland

³Department of Molecular Medicine and Pathology, School of Medical Sciences, The University of Auckland, 1142 Auckland, New Zealand

⁴Division of Haematology, Centre for Cancer Biology, SA Pathology, Adelaide, SA 5000, Australia

⁵Hubrecht Institute-KNAW and UMC Utrecht, 3584CT Utrecht, the Netherlands

⁶Co-senior author

*Correspondence: b.hogan@imb.uq.edu.au

<http://dx.doi.org/10.1016/j.celrep.2014.03.063>

This is an open access article under the CC BY license (<http://creativecommons.org/licenses/by/3.0/>).

SUMMARY

Lymphatic vessels arise during development through sprouting of precursor cells from veins, which is regulated by known signaling and transcriptional mechanisms. The ongoing elaboration of vessels to form a network is less well understood. This involves cell polarization, coordinated migration, adhesion, mixing, regression, and shape rearrangements. We identified a zebrafish mutant, *lymphatic and cardiac defects 1* (*lyc1*), with reduced lymphatic vessel development. A mutation in *polycystic kidney disease 1a* was responsible for the phenotype. *PKD1* is the most frequently mutated gene in autosomal dominant polycystic kidney disease (ADPKD). Initial lymphatic precursor sprouting is normal in *lyc1* mutants, but ongoing migration fails. Loss of *Pkd1* in mice has no effect on precursor sprouting but leads to failed morphogenesis of the subcutaneous lymphatic network. Individual lymphatic endothelial cells display defective polarity, elongation, and adherens junctions. This work identifies a highly selective and unexpected role for *Pkd1* in lymphatic vessel morphogenesis during development.

INTRODUCTION

The lymphatic vasculature forms in the embryo as a result of specification of lymphatic endothelial cell (LEC) fate, followed by coordinated sprouting, morphogenesis, and network elaboration. LEC fate is specified through key transcription factors, which act in embryonic veins (Francois et al., 2008; Srinivasan et al., 2010; Wigle and Oliver, 1999). LEC precursors subsequently sprout from veins and migrate through the embryo (reviewed in Koltowska et al., 2013). This process is under the control of VEGFC/VEGFR3 signaling (Karkkainen et al., 2004)

and its modulators (reviewed in Koltowska et al., 2013). In mouse, lymphatic precursors form lymph sacs in the anterior of the embryo (Francois et al., 2012; Yang et al., 2012), which likely remodel into major lymphatic vessels (Hägerling et al., 2013). Superficial LECs (sLECs) migrate dorsally as loosely attached individual cells to form the subcutaneous lymphatic network (Hägerling et al., 2013). Although several guidance molecules, cellular interactions, and extrinsic forces pattern embryonic lymphangiogenesis (reviewed in Koltowska et al., 2013), much remains to be understood about the cellular mechanisms that regulate LEC polarization, adhesion, outgrowth, remodeling, and morphogenesis.

In zebrafish, there are strong parallels with mammals in the processes that regulate lymphatic vascular development (Hogan et al., 2009b; Küchler et al., 2006; Yaniv et al., 2006). We have used forward genetic screens to identify zebrafish mutants that lack lymphatic vessels. Here, one zebrafish mutant uncovers a surprising role for the ADPKD gene *Pkd1* in lymphatic vascular development. We show that this function of *Pkd1* is conserved and cell autonomous in endothelial knockout mice. Our findings suggest a uniquely staged role for PKD1 in the regulation of lymphatic vascular morphogenesis.

RESULTS

lyc1 Mutants Fail to Form a Lymphatic Vasculature

We identified a zebrafish mutant dubbed *lymphatic and cardiac defects 1* (*lyc1*). *lyc1* mutants exhibited a reduction or loss of the main axial lymphatic vessel, the thoracic duct (TD) at 4 days post-fertilization (dpf) as well as mild cardiac edema, while retaining blood circulation (Figures 1A–1D and 1I). By 5 dpf, mutant blood flow was reduced and cardiac edema increased in severity (Figure S1; data not shown). To determine the origins of the phenotype, we examined gene expression for arteriovenous genes, lymphangiogenesis regulators (including chemokines and receptors), and flow-induced pathways at 32 hr postfertilization (hpf), during the initiation of lymphatic development. These markers were unchanged in *lyc1* embryos (Figure S1). In the zebrafish, precursor

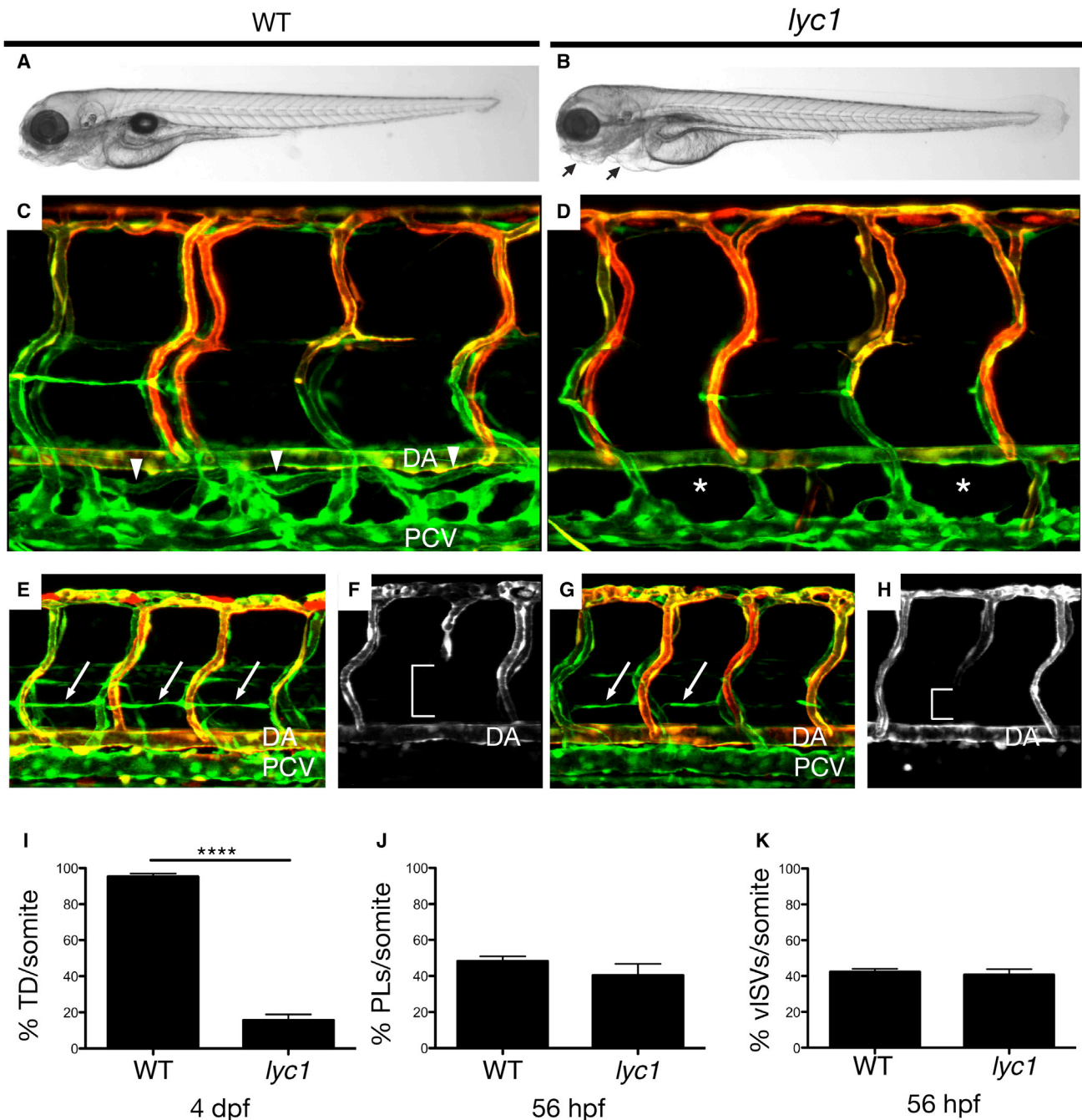


Figure 1. *lyc1* Mutants Display Reduced Lymphatic Development

(A and B) Overall morphology of wild-type siblings (A) and *lyc1* mutants (B) at 4 dpf.

(C and D) The vasculature $Tg(fli1a:EGFP^{Y1}; fli1:tomato^{hu5333Tg})$ of (C) wild-type (WT) (arrowheads indicate thoracic duct) and (D) *lyc1* mutants at 4 dpf (asterisks indicate absence of thoracic duct).

(E and G) The vasculature $Tg(fli1a:EGFP^{Y1}; fli1:tomato^{hu5333Tg})$ in wild-type sibling (E) and mutant embryos (G) at 56 hpf (arrows indicate lymphatic precursors known as parachordal lymphangioblasts, PLs).

(F and H) $fli1:tomato^{hu5333Tg}$ expression marks the arterial ECs, a loss of signal (brackets) indicating venous intersegmental vessels (VISVs).

(I–K) Quantification of (I) thoracic duct extent across ten somites (WT n = 40, *lyc1* n = 17), (J) parachordal lymphangioblasts (WT n = 78, *lyc1* n = 17), and (K) venous sprouts (WT n = 40, *lyc1* n = 15). DA, dorsal aorta; PCV, posterior cardinal vein.

Error bars indicate SEM. See also [Figures S1](#) and [S2](#).

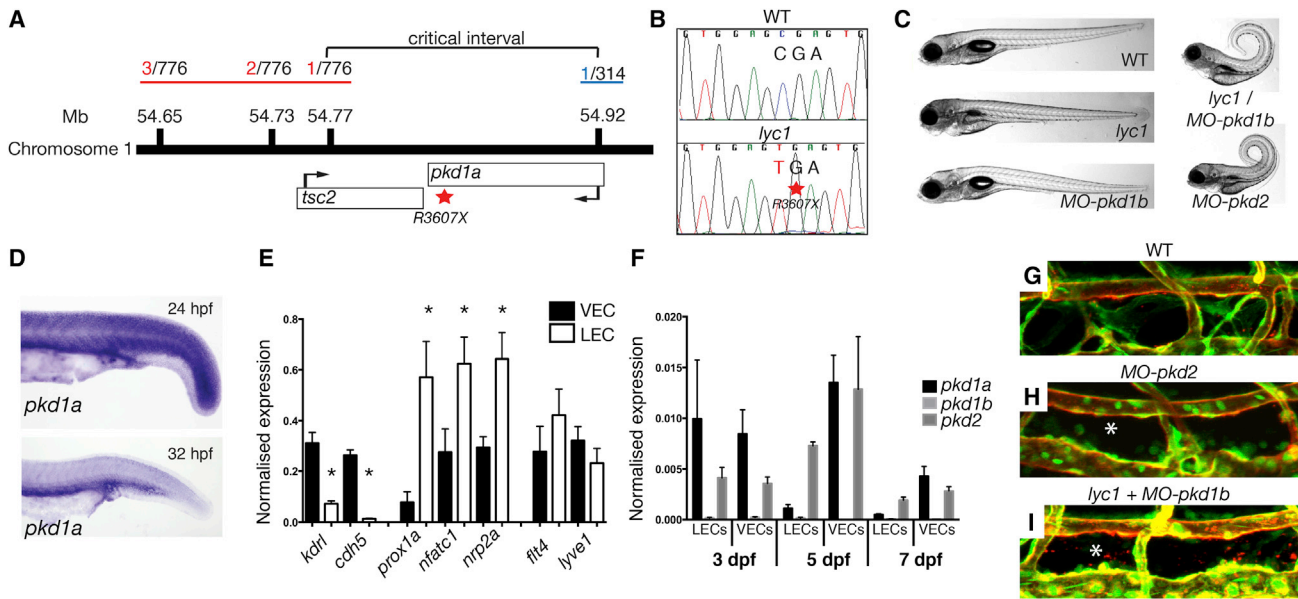


Figure 2. *lyc1* Is a *pkd1a* Mutant

(A) Overview of positional cloning of *lyc1*. Individual recombinant embryos (labeled in red left [from 776 embryos analyzed], labeled in blue right [from 314 embryos analyzed]) identify flanking polymorphic markers and limit the critical interval to a region containing partial sequences for *pkd1a* and *tsc2*. (B) Sequence chromatograms showing the wild-type (upper) and *pkd1a* mutant (R3607X, lower) sequences. (C) Overall morphology of 5 dpf WT, *lyc1*, *MO-pkd1b*, *lyc1/MO-pkd1b*, and *MO-pkd2* embryos. The injection of *MO-pkd1b* into *lyc1* mutants recapitulates the published *MO-pkd1a/1b* double loss-of-function phenotype (Mangos et al., 2010). (D) Expression pattern of *pkd1a* by in situ hybridization in the trunk of wild-type zebrafish at 24 hpf and 32 hpf. (E) Quantitative RT-PCR for markers enriched in venous endothelial cells (VECs); *kdr1*, *cdh5*, LECs; *prox1a*, *nfatc1*, *nrp2a*; and both *flt4* and *lyve1* demonstrated the purity of FACS-isolated populations at 5 dpf. (F) Quantitative RT-PCR for *pkd1a*, *pkd1b*, and *pkd2* transcripts in 3, 5, and 7 dpf VEC and LEC populations. (G–I) The vasculature of 5 dpf WT, *lyc1/MO-pkd1b* and *MO-pkd2* embryos (5 and 7.5 ng MO, respectively); asterisk indicates absence of thoracic duct in *Tg(fli1a:EGFP^{v1}; kdr1:egfp^{s843})* embryos. Error bars indicate SEM. See also Figures S3 and S4.

LECs emerge from the posterior cardinal vein (PCV) during secondary angiogenesis and migrate dorsally to the horizontal myoseptum to form parachordal lymphangioblasts (PLs). Concomitantly, venous sprouts form intersegmental veins (viSVs). Strikingly, the numbers of viSVs and PLs were normal in *lyc1* mutants (Figures 1E–1H, 1J, and 1K).

This phenotype differs from described mutants for *vegfc*, *vegfr3*, or *ccbe1* (Hogan et al., 2009a, 2009b; Le Guen et al., 2014; Villefranc et al., 2013), which lack all venous sprouting. Time-lapse imaging showed that the lymphatic defect resulted from a block in the migration of PLs out of the horizontal myoseptum (Movies S1 and S2). Quantitative analysis of cell behavior spanning this period of altered migration revealed that mutant precursor LECs remain mobile but show altered exploratory behavior and filopodial extension dynamics, consistent with impaired directional migration (Movies S3 and S4; Figure S2).

A Loss-of-Function Mutation in *pkd1a* Is Responsible for the *lyc1* Phenotype

Meiotic mapping (see the Experimental Procedures) was used to identify a region of chromosome 1 containing the *lyc1* locus. The critical interval (Figure 2A) contained two genes, *tuberous sclerosis 2* (*tsc2*) and *polycystic kidney disease la* (*pkd1a*). In the zebrafish genome, *pkd1* (encoding Polycystin1) is present

as duplicate genes, with *pkd1a* coding for a conserved 4281 amino acid protein. Sequencing revealed a mutation in *pkd1a*, introducing a premature stop codon (R3607X) (Figure 2B). This mutation was predicted to result in the failed translation of six of the 11 transmembrane domains and essential C-terminal cytoplasmic tail of the protein.

In humans, *PKD1* and *PKD2* (encoding POLYCYSTIN2) are the most commonly mutated genes in ADPKD (for review, see Chapin and Caplan, 2010; Zhou, 2009). *PKD1* haploinsufficiency and loss of function have also been frequently associated with cardiovascular complications (reviewed in Rossetti and Harris, 2013). In mammals, POLYCYSTIN1 protein localizes to primary cilia, apical membranes, adherens, and desmosomal junctions. It can act as a mechanosensory signaling protein, transducing extracellular signals through its cytoplasmic C-terminal domain (reviewed in Zhou, 2009). POLYCYSTIN1 binds to POLYCYSTIN2 (a calcium pump) at the membrane to regulate Ca^{2+} influx and signaling but also binds to E-cadherin, β -catenin, and components/effectors of the planar cell polarity pathway (Castelli et al., 2013; Lal et al., 2008; Roitbak et al., 2004).

Previous studies depleting Polycystin1 (a and b) in zebrafish found that *MO-pkd1a/b* embryos exhibit a specific body curvature phenotype (Mangos et al., 2010). We injected *MO-pkd1b* into our *pkd1a* mutant embryos and robustly induced this

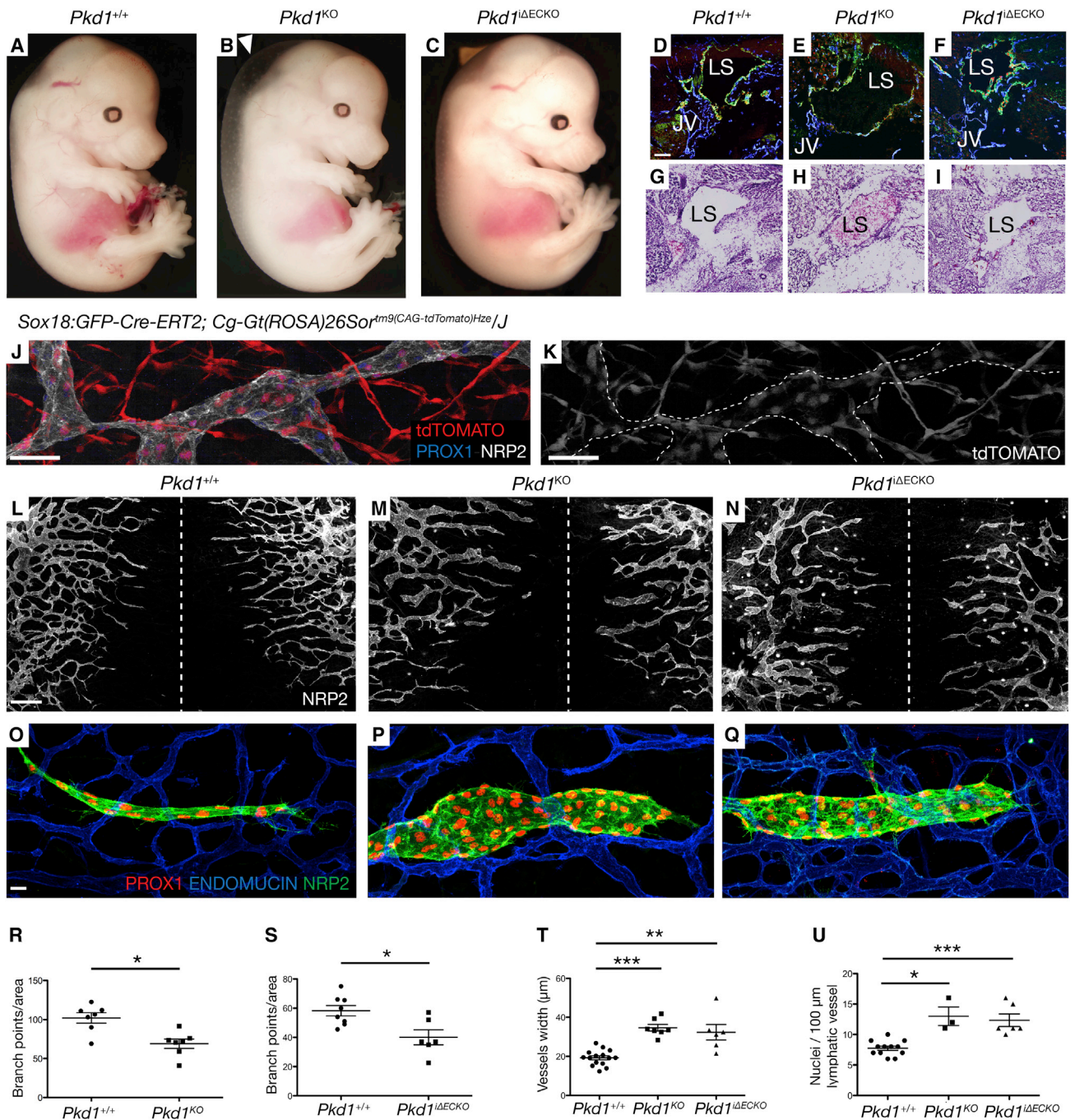


Figure 3. *Pkd1* Cell-Autonomously Regulates Subcutaneous Lymphatic Vascular Development in Mice

(A–C) Morphology of WT, *Pkd1*^{KO}, and *Pkd1*^{ΔECKO} embryos at 14.5 dpc (arrowhead indicates edema).

(D–F) Lymph sacs (LS) in WT, *Pkd1*^{KO}, and *Pkd1*^{ΔECKO} embryos stained with endomucin, LYVE1, and PROX1. JV, jugular vein. Scale bar represents 100 μm.

(G–I) Hematoxylin and eosin staining in WT, *Pkd1*^{KO}, *Pkd1*^{ΔECKO} embryos at 14.5 dpc. Lymph sacs (LS) indicated.

(J and K) Subcutaneous lymphatics in *Sox18:GFP-Cre-ERT2; Cg-Gt(ROSA)26Sor^{tm9(CAG-tdTomato)}Hze/J* costained with NRP2 and PROX1 (n = 663/1,138 scored LECs were tdTOMATO positive (58.2%), from n = 2 embryos, 13.5 dpc).

(L–N) Subcutaneous lymphatic vasculature in WT, *Pkd1*^{KO}, and *Pkd1*^{ΔECKO} mutants at 14.5 dpc. Dashed line indicated the dorsal midline of the embryo. Scale bar represents 400 μm.

(O–Q) Representative subcutaneous lymphatic sprout in WT, *Pkd1*^{KO}, and *Pkd1*^{ΔECKO} mutants at 14.5 dpc.

(R and S) Quantification of branchpoints/area (2,000 × 1,500 μm area on both sides of the midline) in (R) WT (n = 7 embryos) and *Pkd1*^{KO} (n = 7 embryos) and (S) WT (n = 8 embryos) and *Pkd1*^{ΔECKO} (n = 6 embryos) embryos at 14.5 dpc.

(legend continued on next page)

phenotype, confirming that the *lyc1* mutation is a loss-of-function allele (Figures 2C and S3). Pkd1 and Pkd2 can modulate extracellular matrix (ECM) formation (Mangos et al., 2010). Importantly, even the most phenotypically penetrant *pkd1a* mutants for lymphangiogenesis do not display the body curvature associated with altered ECM. We examined several markers and knockdown scenarios but found no evidence for increased ECM or a role of altered matrix in the *lyc1* lymphatic phenotype (Figure S4).

***pkd1a* Is Expressed in Migrating LECs and Loss of Function in the ADPKD Complex Mimics *lyc1* Defects**

We found that *pkd1a* expression was ubiquitous in the 24 hpf embryo but was enriched in the trunk during secondary angiogenesis at 32 hpf (Figure 2D). We saw no evidence for nonsense-mediated decay in mutants using in situ hybridization at 32 hpf ($n = 130$ embryos from a carrier incross analyzed; data not shown). As in situ hybridization has proved insensitive in LECs in older zebrafish (post 3 dpf), we isolated LECs using fluorescence-activated cell sorting (FACS). Taking advantage of a new transgenic line *Tg(lyve1:DsRed2)^{nz101}* (Okuda et al., 2012) labeling embryonic veins and lymphatic vessels, crossed onto the *Tg(kdrl:egfp)^{s843}* line (restricted to blood vessels; Jin et al., 2005), we isolated LECs and venous ECs (VECs). We performed quantitative PCR (qPCR) for known markers, validating the specificity of cell populations (Figures 2E and S3). Consistent with the timing of the *lyc1* phenotype, *pkd1a* and *pkd2* were expressed in VECs and LECs, with *pkd1a* in both populations at 3 dpf but reduced in LECs at 5 dpf. *pkd1b* was expressed at low, almost undetectable levels at all stages (Figures 2F and S3).

In endothelial cells, Polycystin1 can regulate calcium signaling through Polycystin2 activity (Chapin and Caplan, 2010; Nauli et al., 2003). To investigate this potential mechanism, we knocked down Pkd2. Embryos depleted for Pkd2 exhibited a phenotype similar to that of *lyc1/MO-pkd1b* embryos and reduced TD extent (Figures 2G–2I and S3). We next treated embryos with previously validated Ca^{2+} signaling antagonist and agonists (North et al., 2009). These treatments generated phenotypes highly reminiscent of the *lyc1* phenotype (Figure S3). *Cacna1s*, an L-type calcium channel targeted by the antagonist Nifedipine, was expressed in ECs (Figure S3). Taken together, these observations are consistent with Pkd1 functioning in the canonical ADPKD complex.

***Pkd1* Cell-Autonomously Regulates Development of the Subcutaneous Lymphatic Vascular Network in Mice**

Although most previous studies in mammalian models focus on the role of *Pkd1* in epithelia, *Pkd1*-null mice have been shown to exhibit cardiovascular, skeletal, and renal defects (Boulter et al., 2001; Kim et al., 2000; Piontek et al., 2004). Embryos devoid of *Pkd1* die after 15.5 days post coitum (dpc) displaying severe

hemorrhaging and subcutaneous edema (Kim et al., 2000; Muto et al., 2002), but a role for this gene in lymphangiogenesis has yet to be reported.

We generated *Pkd1* knockout embryos and examined their overall morphology. We observed the previously described subcutaneous edema, but not hemorrhaging (Figures 3A–3C). Embryonic lymph sacs were present but were blood filled in *Pkd1* KO embryos (Figures 3D–3I). This phenotype suggests that lymphatics in this mutant would not sustain fluid drainage and may explain the subcutaneous edema. Interestingly, we did not find any defect in lymphovenous valves at 14.5 dpc (Figure S5) perhaps suggesting that blood enters the mutant lymph sacs early during morphogenesis, before valve maturation (François et al., 2012). We next examined the developing subcutaneous lymphatic vasculature in dorsal embryonic skin, a useful system to quantify lymphatic vascular phenotypes (James et al., 2013; Kartopawiro et al., 2014). We found that *Pkd1* KO embryos exhibit defects in the morphogenesis of the lymphatic network, with increased width of sprouting vessels, increased cell number per vessel, and a significant reduction in network branching (Figures 3L, 3M, 3R, 3T, and 3U).

Previous studies reported that *Tie2:Cre*-mediated deletion of *Pkd1* did not lead to vascular abnormalities, and these knockout mice did not display the edema observed in full knockout animals (Garcia-Gonzalez et al., 2010; Hassane et al., 2011). This implies that the phenotypes that we observed may not reflect endothelial autonomous function. To investigate this further, we crossed the *Tie2:Cre* strain into a *ROSA26r-LacZ* background and examined Cre activity. Although active in blood vessels, we could not detect activity throughout subcutaneous lymphatic vessels (Figure S6). Hence, previous work would not have uncovered function in these vessels. We generated *Tie2:Cre*-mediated knockout embryos for *Pkd1* and found no subcutaneous lymphatic phenotype (Figure S5). Therefore, we utilized *Sox18:GFP-Cre-Ert2(GCE)* as an additional endothelial CRE strain (Kartopawiro et al., 2014). We validated the use of *Sox18:GCE* on a *Rosa26r-LacZ* background, which demonstrated activity throughout the vasculature (Figure S6). We also used an inducible *tdTomato* reporter to quantify activity in subcutaneous lymphatics by costaining with LEC markers NRP2 and PROX1. We found that induced *Sox18:GCE* was active in 58% of sprouting subcutaneous LECs at 13.5 dpc and frequently in clonal regions spanning whole vessels (Figures 3J, 3K, and S6H–S6Q; Movie S5).

We generated induced *Pkd1* endothelial cell knockout ($i\Delta ECKO$) embryos using this line. *Pkd1^{i\Delta ECKO}* embryos displayed either mild or no subcutaneous edema at 14.5 dpc (Figure 3C), with lymph sacs present but not containing blood (Figures 3I and 3F). In the subcutaneous lymphatic vasculature, *Pkd1^{i\Delta ECKO}* embryos displayed similar dramatic defects to germline KO animals, if marginally milder on quantification (Figures

(T) Quantification of the average width of lymphatic vessels (μm) across the whole skin in WT ($n = 15$ embryos), *Pkd1^{KO}* ($n = 7$ embryos), and *Pkd1^{i\Delta ECKO}* ($n = 6$ embryos) embryos. The average is shown of $n = 773$, $n = 354$, and $n = 250$ measurements, respectively, across leading lymphatic vessels from both sides of the midline at 14.5 dpc.

(U) Quantification of nuclei/100 μm of vessel in WT ($n = 12$ embryos), *Pkd1^{KO}* ($n = 3$ embryos), and *Pkd1^{i\Delta ECKO}* ($n = 6$ embryos) ($n = 5$ representative leading edge vessels counted per embryo) at 14.5 dpc.

Error bars indicate SEM. See also Figures S5 and S6.

3N, 3Q, 3T, and 3U). We examined the blood vasculature of *Pkd1* KO embryos. Although we saw defects in *Pkd1*^{KO} embryos, these were at the dorsal midline associated with edema and considered secondary to altered tissue architecture (Figure S5). In contrast, *Pkd1*^{ΔECKO} embryos displayed normal blood vasculature, including normal vessel width and branching (Figure S5). Interestingly, *Pkd1*^{ΔECKO} embryos did not show reduced LEC migration toward the midline (Figure 3N). This would be expected for mutants in known pathways such as VEGFC/VEGFR3.

PKD1 Regulates Sprouting and Cell-Cell Junctions In Vitro in Human LECs

Next, we examined the sprouting of human LECs in vitro in response to VEGFC using a spheroid outgrowth assay. Small interfering RNA (siRNA)-mediated knockdown of *PKD1* in LECs resulted in a reduced number of cells within individual spheroid sprouts, with extensions exhibiting reduced length and abnormal morphology (Figures 4A–4H; Figure S7). The efficacy of knockdown with the siRNA mix was validated by qPCR, and the specificity was verified with an independent small hairpin RNA (shRNA) knockdown (Figure S7). We examined the phenotype of LECs in cultured monolayers and observed a rapid change in morphology following *PKD1* knockdown (Figures 4I–4P). Stress fibers were disorganized in these cells (Figures 4I and 4M), and analysis of cell junctions revealed reduced VE-cadherin and β-catenin and disorganized junctions following knockdown (Figures 4J, 4K, 4N, and 4O). ZO-1 localization at tight junctions was relatively unaffected in these assays, despite altered cell morphology, suggesting a level of selectivity to adherens junctions (Figures 4L and 4P). The levels of VE-cadherin were not altered by western blot although β-catenin showed a mild reduction (Figure S7), probably indicative of destabilized junctional complexes.

Pkd1 Regulates Polarity and Cell-Cell Junctions during Lymphatic Vessel Morphogenesis in Mice

Pkd1 has been implicated in the regulation of polarity in epithelial cells and shown to regulate cellular convergent extension and polarity during kidney tubule morphogenesis through planar cell polarity (PCP) signaling (Castelli et al., 2013). PKD1 binds to PAR3 and aPKC as well as E-cadherin and β-catenin therefore being associated with both polarity and junctional components (Castelli et al., 2013; Lal et al., 2008; Roitbak et al., 2004). Recently, the PCP pathway has been shown to regulate junctional rearrangements in developing LECs, at least during valve morphogenesis (Tatin et al., 2013).

We examined cell polarity in sprouting embryonic lymphatic vessels. The Golgi apparatus orients toward the migration front relative to the nucleus in many cell types including LECs (Figures 5A and 5C), serving as an ideal readout for polarity. We quantified Golgi orientation in *Pkd1* KO embryos and found it to be significantly randomized in 14.5 dpc lymphatic vessels compared with siblings (Figures 5A–5D and 5G). Furthermore, this loss of polarity was associated with increased nucleus sphericity in mutant vessels, a previously described proxy for polarity and migratory behavior (Hägerling et al., 2013) (Figure 5H).

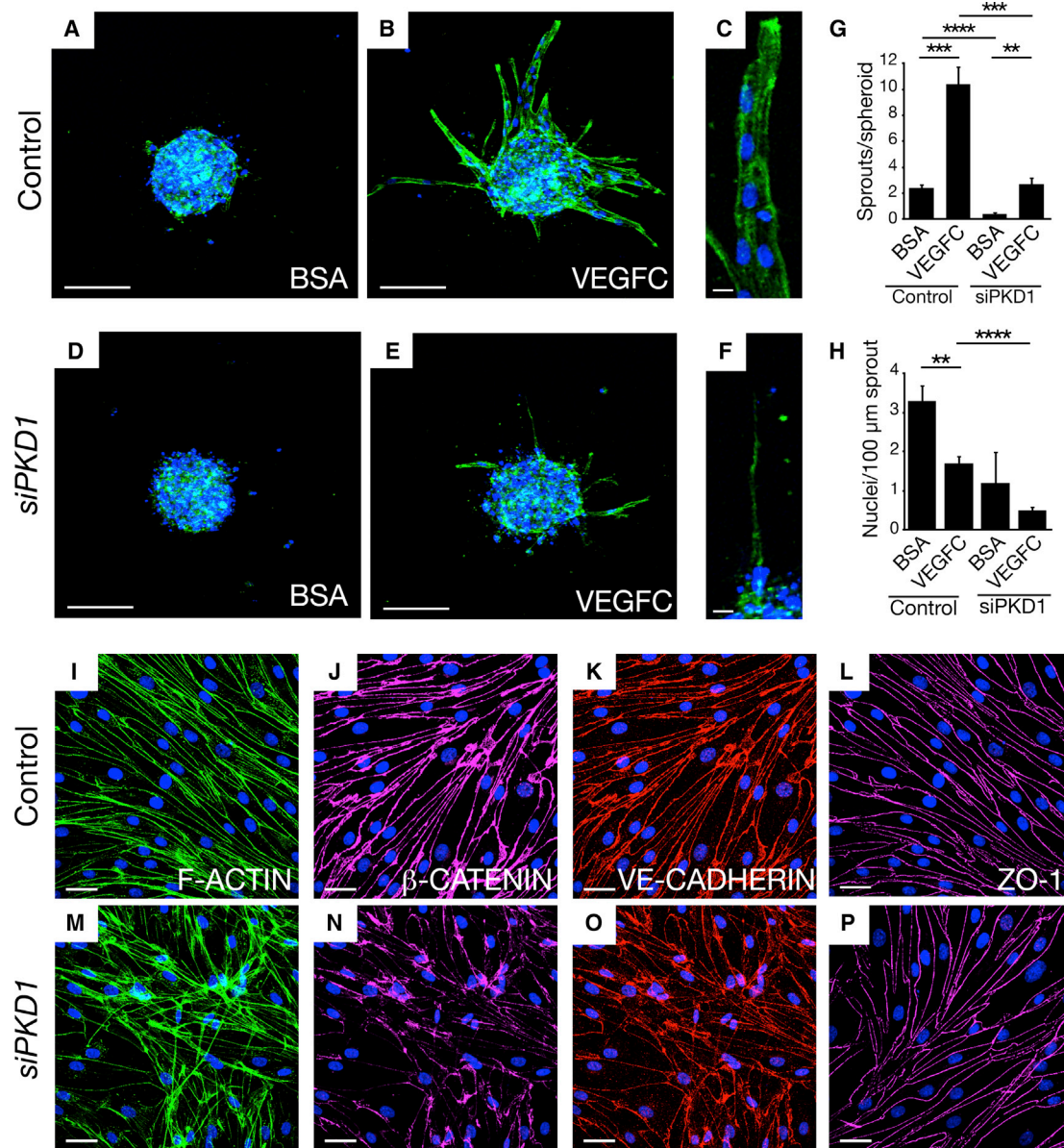
To determine the earliest defect, we performed detailed phenotypic analysis at 10.5 and 11.5 dpc. At 10.5 dpc, analysis of PROX1 expression indicated that cell migration from the cardinal vein and nuclear morphology was normal in mutants (Figures 5I, S6G, and S6H). However, at 11.5 dpc, although the blood vasculature was grossly normal (Figure S5), mutant LECs at the sprouting vessel front displayed increased nucleus sphericity (decreased ellipticity) compared with wild-type (Figure 5J). We assessed Golgi orientation at these stages, but the direction of individual cell migration events was not regular, and the midline cannot be used as a direction of migration until later in development (data not shown). These early leading vessels also exhibited increased width and numbers of nuclei relative to vessel length similar to later *Pkd1*^{KO} vessels (Figures S5I–S5J).

Finally, we investigated cell shape and the morphology of junctions within lymphatic vessels. At 14.5 dpc, VE-cadherin highlighted cell shape and showed that mutant cells failed to elongate along the plane of migration toward the midline compared with wild-type vessels (Figures 5K, 5L, 5O, 5P, and 5S). At the level of individual junctional morphology, both VE-cadherin and β-catenin expression identified junctions that displayed immature morphology with irregular intracellular protrusions (arrowheads in Figures 5M, 5N, 5Q, and 5R). These phenotypes were only seen in phenotypically mutant vessels and not morphologically wild-type mutant vessels (data not shown; phenotypic variability shown in Figure 3). Quantification of the number of cells displaying immature junctions showed a significant phenotype from as early as 12.5 dpc (Figures 5T–5V).

DISCUSSION

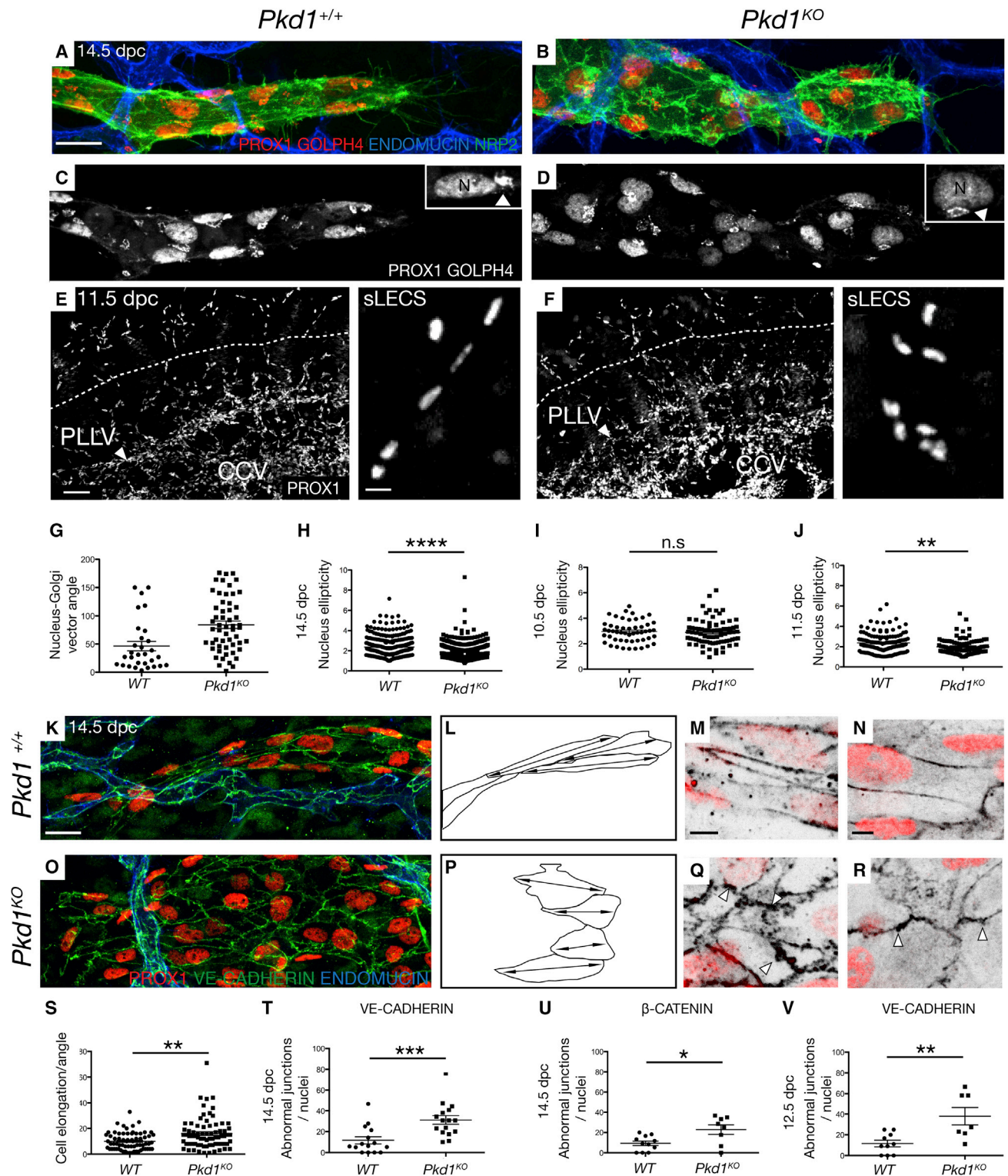
Our results, along with those of Outeda et al. (2014) published in this issue of *Cell Reports* demonstrate the surprising finding that *Pkd1* is a regulator of lymphatic vessel development. In zebrafish, at the cellular level, *Pkd1* regulates LEC migration out of the horizontal myoseptum but not initial sprouting from veins that is regulated by *ccbe1/vegfc/vegfr3* (Hogan et al., 2009a, 2009b; Le Guen et al., 2014; Villefranc et al., 2013). *pkd1a* is expressed in lymphatic precursor cells when they are actively migrating, consistent with the earliest cellular defects in the mutant.

It was important, given the highly studied nature of *Pkd1*, to ask if this function was conserved in mammals. In knockout mice, early specification and initial sprouting of LECs occurs normally. However, defects are seen in the morphology of migrating LECs at 11.5 dpc with morphological defects in the subcutaneous lymphatic network prominent by 14.5 dpc. This uniquely timed requirement is distinct from phenotypes in known pathways, suggesting that *Pkd1* may act by an uncharacterized mechanism in LECs. Interestingly, the lymph sacs were blood filled in full knockout but not in endothelial knockout mice, which displayed only mild edema. This may be due to the staging of tamoxifen treatment to knockout *Pkd1* function from 9.5 or 11.5 dpc, when lymph sacs are already establishing (Hägerling et al., 2013). The observation that the lymphatic phenotype was reproduced by deletion with *Sox18:GCE*, active in LECs, but not *Tie2:Cre*, which we observed acts in BECs, suggests that *Pkd1* functions in the LECs themselves during vessel morphogenesis.



Given the diverse functions of the protein, several hypotheses could explain the observed migration and morphogenesis defects. PKD1 has been previously reported to function at the primary cilium in endothelial cells (Nauli et al., 2008). However, we found lymphatic vessels developed normally in a ciliogenesis mutant (*ift88*; Huang and Schier, 2009), we saw no evidence for altered ciliogenesis in *lyc1* mutants, and overexpression of

a Pkd1a-YFP fusion protein, driven by the *pkd1a* promoter (BAC clone), did not lead to cilium enrichment (Figure S8). Hence, we find no supportive evidence that Pkd1 in zebrafish lymphatic development functions at the cilium. Because Pkd1 can also localize to adherens junctions, desmosomal junctions, and intracellular organelles and has a number of binding partners, it has the potential to act at diverse locations.



(legend continued on next page)

The earliest consequences of loss of function are changes in cell morphology during morphogenesis, including altered polarity and adhesion. Cell polarity and adhesion are intimately associated and must be carefully regulated to control tissue morphogenesis. It is hard to determine which defect is primarily regulated by *Pkd1*. However, parallels can be drawn with recent findings in kidney tubule development where *Pkd1* regulates cellular convergent extension during tube formation through the PCP pathway (Castelli et al., 2013). Although it will take further work to delineate the pathways modulated by *Pkd1* in LECs, the finding of a crucial role in lymphatic vascular development is unexpected and serves as a unique entry point to understand lymphatic vascular morphogenesis.

EXPERIMENTAL PROCEDURES

Zebrafish Strains, Mapping, and Genotyping

Animal use conformed to guidelines of the animal ethics committee at the University of Queensland. Zebrafish were maintained and screening performed as previously described (Hogan et al., 2009a). Mapping and genotyping was performed as previously described (Hogan et al., 2009a). Primers are given in Supplemental Experimental Procedures. The *lyc1* mutant allele is formally designated *pkd1a*^{hu5855}. The *Tg(flt1:YFP)*^{hu4624Tg}, *Tg(kdrl:egfp)*^{s843}, *Tg(fli1a:EGFP)*^{y1}, *Tg(-6.5kdrl:mcherry)*^{s916}, *Tg(-0.8flt1:tdTomato)*^{hu5333Tg}, and *Tg(lyve1:DsRed2)*^{nz101} lines were previously described (Bussmann et al., 2010; Hogan et al., 2009b; Jin et al., 2005; Krueger et al., 2011; Lawson and Weinstein, 2002; Okuda et al., 2012).

Mouse Strains

We generated *Sox18:GFP-Cre-Ert2(GCE)*, *B6.129S4-Pkd1^{tm2Ggg/J} (Pkd1^{fl/fl}); Rosa26rLacZ* (C57BL/6 background) mice by crossing *Pkd1^{fl/fl}* mice to both *Rosa26rLacZ* and *Sox18:GFP-Cre-Ert2* mice and breeding resulting carriers. We generated *Tie2:Cre*, *Rosa26rLacZ* (C57BL/6 background) mice by crossing *Tie2:Cre* mice to *Rosa26rLacZ* and breeding resulting carriers. We generated *Sox18:GFP-Cre-Ert2(GCE)*, *Cg-Gt(ROSA)26Sor^{tm9(CAG-tdTomato)Hze/J}* by crossing *Sox18:GFP-Cre-Ert2* mice to *Cg-Gt(ROSA)26Sor^{tm9(CAG-tdTomato)Hze/J}* homozygous mice. We generated *Pkd1^{-/-}* embryos by crossing *Pkd1^{fl/fl}* mice to *B6.C-Tg(CMV-cre)1Cgn/J* and inbreeding resulting progeny in subsequent generations. Genotyping primers are described in Supplemental Experimental Procedures.

Imaging and Analysis

For confocal and spinning disk imaging, embryos were mounted as previously described (Hogan et al., 2009b). Imaging was performed on a LSM Zeiss 510 NLO, META, or Zeiss 710 FCS confocal microscope with a 10×, 20×, and 40× dry objective and 63× oil objective. Images were analyzed with the Zen software, Biplane IMARIS, Photoshop, and ImageJ.

Morpholino Oligomers

Morpholino oligomers against *pkd1a* (morpholino oligomer [MO] ex8), *pkd1b* (MO ex45), and *pkd2* (MO ATG) were described in Mangos et al. (2010) and were injected at 5, 7.5, or 10 ng/embryo as described (Hogan et al., 2008).

Quantitative Real-Time PCR

Procedures were performed in order to comply with MIQE guidelines (Bustin et al., 2009) and are given in full in Supplemental Experimental Procedures.

SUPPLEMENTAL INFORMATION

Supplemental Information includes Supplemental Experimental Procedures, eight figures, one table, and five movies and can be found with this article online at <http://dx.doi.org/10.1016/j.celrep.2014.03.063>.

AUTHOR CONTRIBUTIONS

B.C. performed experiments, analyzed data, and cowrote the paper; A.S., N.I.B., K.A.S., C.P.-T., R.S., J.W.A., E.F., and M.J. performed experiments and analyzed data; P.S.C., R.G.P., N.L.H., T.V.P., and S.S.-M. designed experiments, analyzed data, and edited the paper; M.F. designed experiments, performed experiments, analyzed data, and edited the paper; B.M.H. designed experiments, performed experiments, analyzed data, and cowrote the paper.

ACKNOWLEDGMENTS

We thank Christine Neyt, Scott Paterson, Nicole Schieber, and Merlijn Witte for technical assistance and Carol Wicking for useful discussions. We thank Holger Gerhardt for providing protocols, GUDMAP consortium for *Sox18:GCE*, and the Baltimore PKD Core for the *PKD1* shRNAs. B.M.H. was funded by an Australian Research Council Future Fellowship (FT100100165), M.F. by an NHMRC Australia Career Development Fellowship (1011242), K.A.S. by an Australian Research Council Future Fellowship (FT10100496), and R.G.P. by an NHMRC Australia Fellowship (569542). This work was funded

(E and F) Lateral view of (E) WT (n = 3) and (F) *Pkd1^{KO}* (n = 2) bisected embryos with PROX1 at 11.5 dpc. CCV, common cardinal vein. Right panels show morphology of migrating sLEC nuclei (analyzed above dashed line). Scale bar represents 50 μ m (10 μ m in right-hand panels).
 (G and H) Quantification of nucleus-Golgi vector angle (G) in WT (n = 3 embryos, n = 30 nuclei) and *Pkd1^{KO}* (n = 4, n = 55 nuclei) and (H) quantification of nucleus sphericity (width to length ratio) in WT (n = 7, n = 299 nuclei) and *Pkd1^{KO}* (n = 7, n = 498 nuclei) at 14.5 dpc.
 (I and J) Quantification of nucleus sphericity in (I) dorsal-most iLECs in WT (n = 5, n = 51 nuclei) versus *Pkd1^{KO}* (n = 5, n = 79 nuclei) embryos at 10.5 dpc, (J) in sLECs in WT (n = 3, n = 131 nucleus) and *Pkd1^{KO}* (n = 2, n = 93 nucleus) embryos at 11.5 dpc
 (K and O) Representative subcutaneous lymphatic vessels in (K) WT and (O) *Pkd1^{KO}* embryos stained with endomucin, PROX1, and VE-cadherin at 14.5 dpc. Scale bar represents 20 μ m
 (L and P) Representative cell shape schematics based on vessels shown in (K) and (O) show abnormal elongation in the direction of vessel migration. Double-sided arrows indicate elongation axes.
 (M and Q) WT and *Pkd1^{KO}* mutant cells at 14.5 dpc stained with PROX1 and VE-cadherin. Arrowheads indicate abnormal junctional protrusions. Scale bar represents 5 μ m.
 (N and R) WT and *Pkd1^{KO}* mutant cells at 14.5 dpc stained with PROX1 and β -catenin. Arrowheads indicate abnormal junctional protrusions. Scale bar represents 5 μ m.
 (S) Quantification of the angle of cell elongation relative to the direction of migration in WT (n = 68 cells, n = 4 embryos) and *Pkd1^{KO}* (n = 74 cells, n = 4 embryos).
 (T) Quantification of the average number of cells with abnormal junctions (stained with VE-cadherin) per nuclei in WT (n = 4 embryos, n = 15 vessels) and *Pkd1^{KO}* (n = 4 embryos, n = 16 vessels) at 14.5 dpc.
 (U) Quantification of abnormal junctions (stained with β -catenin) in WT (n = 3 embryos, n = 11 vessels) and *Pkd1^{KO}* (n = 2 embryos, n = 8 vessels) at 14.5 dpc.
 (V) Quantification of the average number of cells with abnormal junctions (stained with VE-cadherin) per nuclei in WT (n = 4 embryos, n = 10 vessels) and *Pkd1^{KO}* (n = 3 embryos, n = 7 vessels) at 12.5 dpc.
 iLECS, initial LECs; PLLV, peripheral longitudinal lymphatic vessel; sLECS, superficial LECs; CCV, common cardinal vein. Error bars indicate SEM.

by Cancer Council Queensland project grant (1043659) and in part by NHMRC project grant (631657). J.W.A. was funded by the Auckland Medical Research Foundation. Imaging was performed in the Australian Cancer Research Foundation's Dynamic Imaging Facility at IMB.

Received: July 22, 2013
Revised: February 13, 2014
Accepted: March 26, 2014
Published: April 24, 2014

REFERENCES

- Boulter, C., Mulroy, S., Webb, S., Fleming, S., Brindle, K., and Sandford, R. (2001). Cardiovascular, skeletal, and renal defects in mice with a targeted disruption of the Pkd1 gene. *Proc. Natl. Acad. Sci. USA* **98**, 12174–12179.
- Bussmann, J., Bos, F.L., Urasaki, A., Kawakami, K., Duckers, H.J., and Schulte-Merker, S. (2010). Arteries provide essential guidance cues for lymphatic endothelial cells in the zebrafish trunk. *Development* **137**, 2653–2657.
- Bustin, S.A., Benes, V., Garson, J.A., Hellems, J., Huggett, J., Kubista, M., Mueller, R., Nolan, T., Pfaffl, M.W., Shipley, G.L., et al. (2009). The MIQE guidelines: minimum information for publication of quantitative real-time PCR experiments. *Clin. Chem.* **55**, 611–622.
- Castelli, M., Boca, M., Chiaravalli, M., Ramalingam, H., Rowe, I., Distefano, G., Carroll, T., and Boletta, A. (2013). Polycystin-1 binds Par3/aPKC and controls convergent extension during renal tubular morphogenesis. *Nat Commun* **4**, 2658.
- Chapin, H.C., and Caplan, M.J. (2010). The cell biology of polycystic kidney disease. *J. Cell Biol.* **191**, 701–710.
- François, M., Caprini, A., Hosking, B., Orsenigo, F., Wilhelm, D., Browne, C., Paavonen, K., Karnezis, T., Shayan, R., Downes, M., et al. (2008). Sox18 induces development of the lymphatic vasculature in mice. *Nature* **456**, 643–647.
- François, M., Short, K., Secker, G.A., Combes, A., Schwarz, Q., Davidson, T.-L., Smyth, I., Hong, Y.-K., Harvey, N.L., and Koopman, P. (2012). Segmental territories along the cardinal veins generate lymph sacs via a ballooning mechanism during embryonic lymphangiogenesis in mice. *Dev. Biol.* **364**, 89–98.
- Garcia-Gonzalez, M.A., Outeda, P., Zhou, Q., Zhou, F., Menezes, L.F., Qian, F., Huso, D.L., Germino, G.G., Piontek, K.B., and Watnick, T. (2010). Pkd1 and Pkd2 are required for normal placental development. *PLoS ONE* **5**, 5.
- Hägerling, R., Pollmann, C., Andreas, M., Schmidt, C., Nurmi, H., Adams, R.H., Alitalo, K., Andresen, V., Schulte-Merker, S., and Kiefer, F. (2013). A novel multistep mechanism for initial lymphangiogenesis in mouse embryos based on ultramicroscopy. *EMBO J.* **32**, 629–644.
- Hassane, S., Claij, N., Jodar, M., Dedman, A., Lauritzen, I., Duprat, F., Koenderman, J.S., van der Wal, A., Breuning, M.H., de Heer, E., et al. (2011). Pkd1-inactivation in vascular smooth muscle cells and adaptation to hypertension. *Lab. Invest.* **91**, 24–32.
- Hogan, B.M., Verkade, H., Lieschke, G.J., and Heath, J.K. (2008). Manipulation of gene expression during zebrafish embryonic development using transient approaches. *Methods Mol. Biol.* **469**, 273–300.
- Hogan, B.M., Bos, F.L., Bussmann, J., Witte, M., Chi, N.C., Duckers, H.J., and Schulte-Merker, S. (2009a). Ccbe1 is required for embryonic lymphangiogenesis and venous sprouting. *Nat. Genet.* **41**, 396–398.
- Hogan, B.M., Herpers, R., Witte, M., Heloterä, H., Alitalo, K., Duckers, H.J., and Schulte-Merker, S. (2009b). Vegfc/Flt4 signalling is suppressed by Dll4 in developing zebrafish intersegmental arteries. *Development* **136**, 4001–4009.
- Huang, P., and Schier, A.F. (2009). Dampened Hedgehog signaling but normal Wnt signaling in zebrafish without cilia. *Development* **136**, 3089–3098.
- James, J.M., Nalbandian, A., and Mukoyama, Y.S. (2013). TGF β signaling is required for sprouting lymphangiogenesis during lymphatic network development in the skin. *Development* **140**, 3903–3914.
- Jin, S.W., Beis, D., Mitchell, T., Chen, J.N., and Stainier, D.Y. (2005). Cellular and molecular analyses of vascular tube and lumen formation in zebrafish. *Development* **132**, 5199–5209.
- Karkkainen, M.J., Haiko, P., Sainio, K., Partanen, J., Taipale, J., Petrova, T.V., Jeltsch, M., Jackson, D.G., Talikka, M., Rauvala, H., et al. (2004). Vascular endothelial growth factor C is required for sprouting of the first lymphatic vessels from embryonic veins. *Nat. Immunol.* **5**, 74–80.
- Kartopawiro, J., Bower, N.I., Karnezis, T., Kazenwadel, J., Betterman, K.L., Lesieur, E., Koltowska, K., Astin, J., Crosier, P., Vermeren, S., et al. (2014). Arap3 is dysregulated in a mouse model of hypotrichosis-lymphedema-telangiectasia and regulates lymphatic vascular development. *Hum. Mol. Genet.* **23**, 1286–1297.
- Kim, K., Drummond, I., Ibraghimov-Beskrovnaya, O., Klinger, K., and Arnaout, M.A. (2000). Polycystin 1 is required for the structural integrity of blood vessels. *Proc. Natl. Acad. Sci. USA* **97**, 1731–1736.
- Koltowska, K., Betterman, K.L., Harvey, N.L., and Hogan, B.M. (2013). Getting out and about: the emergence and morphogenesis of the vertebrate lymphatic vasculature. *Development* **140**, 1857–1870.
- Krueger, J., Liu, D., Scholz, K., Zimmer, A., Shi, Y., Klein, C., Siekmann, A., Schulte-Merker, S., Cudmore, M., Ahmed, A., and le Noble, F. (2011). Flt1 acts as a negative regulator of tip cell formation and branching morphogenesis in the zebrafish embryo. *Development* **138**, 2111–2120.
- Küchler, A.M., Gjini, E., Peterson-Maduro, J., Cancilla, B., Wolburg, H., and Schulte-Merker, S. (2006). Development of the zebrafish lymphatic system requires VEGFC signaling. *Curr. Biol.* **16**, 1244–1248.
- Lal, M., Song, X., Pluznick, J.L., Di Giovanni, V., Merrick, D.M., Rosenblum, N.D., Chauvet, V., Gottardi, C.J., Pei, Y., and Caplan, M.J. (2008). Polycystin-1 C-terminal tail associates with beta-catenin and inhibits canonical Wnt signaling. *Hum. Mol. Genet.* **17**, 3105–3117.
- Lawson, N.D., and Weinstein, B.M. (2002). In vivo imaging of embryonic vascular development using transgenic zebrafish. *Dev. Biol.* **248**, 307–318.
- Le Guen, L., Karpanen, T., Schulte, D., Harris, N.C., Koltowska, K., Roukens, G., Bower, N.I., van Impel, A., Stacker, S.A., Achen, M.G., et al. (2014). Ccbe1 regulates Vegfc-mediated induction of Vegfr3 signaling during embryonic lymphangiogenesis. *Development* **141**, 1239–1249.
- Mangos, S., Lam, P.Y., Zhao, A., Liu, Y., Mudumana, S., Vasilyev, A., Liu, A., and Drummond, I.A. (2010). The ADPKD genes pkd1a/b and pkd2 regulate extracellular matrix formation. *Dis. Model. Mech.* **3**, 354–365.
- Muto, S., Aiba, A., Saito, Y., Nakao, K., Nakamura, K., Tomita, K., Kitamura, T., Kurabayashi, M., Nagai, R., Higashihara, E., et al. (2002). Pioglitazone improves the phenotype and molecular defects of a targeted Pkd1 mutant. *Hum. Mol. Genet.* **11**, 1731–1742.
- Nauli, S.M., Alenghat, F.J., Luo, Y., Williams, E., Vassilev, P., Li, X., Elia, A.E., Lu, W., Brown, E.M., Quinn, S.J., et al. (2003). Polycystins 1 and 2 mediate mechanosensation in the primary cilium of kidney cells. *Nat. Genet.* **33**, 129–137.
- Nauli, S.M., Kawanabe, Y., Kaminski, J.J., Pearce, W.J., Ingber, D.E., and Zhou, J. (2008). Endothelial cilia are fluid shear sensors that regulate calcium signaling and nitric oxide production through polycystin-1. *Circulation* **117**, 1161–1171.
- North, T.E., Goessling, W., Peeters, M., Li, P., Ceol, C., Lord, A.M., Weber, G.J., Harris, J., Cutting, C.C., Huang, P., et al. (2009). Hematopoietic stem cell development is dependent on blood flow. *Cell* **137**, 736–748.
- Okuda, K.S., Astin, J.W., Misa, J.P., Flores, M.V., Crosier, K.E., and Crosier, P.S. (2012). Iyve1 expression reveals novel lymphatic vessels and new mechanisms for lymphatic vessel development in zebrafish. *Development* **139**, 2381–2391.
- Outeda, P., Huso, D.L., Fisher, S.A., Halushka, M.K., Kim, H., Qian, F., Germino, G.G., and Watnick, T. (2014). Polycystin signaling is required for directed endothelial cell migration and lymphatic development. *Cell Rep.* **7**, Published online April 24, 2014. <http://dx.doi.org/10.1016/j.celrep.2014.03.064>.
- Piontek, K.B., Huso, D.L., Grinberg, A., Liu, L., Bedja, D., Zhao, H., Gabrielson, K., Qian, F., Mei, C., Westphal, H., and Germino, G.G. (2004). A functional

- floxed allele of *Pkd1* that can be conditionally inactivated in vivo. *J. Am. Soc. Nephrol.* *15*, 3035–3043.
- Roitbak, T., Ward, C.J., Harris, P.C., Bacallao, R., Ness, S.A., and Wandinger-Ness, A. (2004). A polycystin-1 multiprotein complex is disrupted in polycystic kidney disease cells. *Mol. Biol. Cell* *15*, 1334–1346.
- Rossetti, S., and Harris, P.C. (2013). The genetics of vascular complications in autosomal dominant polycystic kidney disease (ADPKD). *Curr. Hypertens. Rep.* *9*, 37–43.
- Srinivasan, R.S., Geng, X., Yang, Y., Wang, Y., Mukatira, S., Studer, M., Porto, M.P., Lagutin, O., and Oliver, G. (2010). The nuclear hormone receptor Coup-TFII is required for the initiation and early maintenance of *Prox1* expression in lymphatic endothelial cells. *Genes Dev.* *24*, 696–707.
- Tatin, F., Taddei, A., Weston, A., Fuchs, E., Devenport, D., Tissir, F., and Makinen, T. (2013). Planar cell polarity protein *Celsr1* regulates endothelial adherens junctions and directed cell rearrangements during valve morphogenesis. *Dev. Cell* *26*, 31–44.
- Villefranc, J.A., Nicoli, S., Bentley, K., Jeltsch, M., Zarkada, G., Moore, J.C., Gerhardt, H., Alitalo, K., and Lawson, N.D. (2013). A truncation allele in vascular endothelial growth factor *c* reveals distinct modes of signaling during lymphatic and vascular development. *Development* *140*, 1497–1506.
- Wigle, J.T., and Oliver, G. (1999). *Prox1* function is required for the development of the murine lymphatic system. *Cell* *98*, 769–778.
- Yang, Y., Garcia-Verdugo, J.M., Soriano-Navarro, M., Srinivasan, R.S., Scallan, J.P., Singh, M.K., Epstein, J.A., and Oliver, G. (2012). Lymphatic endothelial progenitors bud from the cardinal vein and intersomitic vessels in mammalian embryos. *Blood* *120*, 2340–2348.
- Yaniv, K., Isogai, S., Castranova, D., Dye, L., Hitomi, J., and Weinstein, B.M. (2006). Live imaging of lymphatic development in the zebrafish. *Nat. Med.* *12*, 711–716.
- Zhou, J. (2009). Polycystins and primary cilia: primers for cell cycle progression. *Annu. Rev. Physiol.* *71*, 83–113.

Cell Reports, Volume 7

Supplemental Information

Pkd1 Regulates Lymphatic Vascular

Morphogenesis during Development

Baptiste Coxam, Amélie Sabine, Neil I. Bower, Kelly A. Smith, Cathy Pichol-Thievend, Renae Skoczylas, Jonathan W. Astin, Emmanuelle Frampton, Muriel Jaquet, Philip S. Crosier, Robert G. Parton, Natasha L. Harvey, Tatiana V. Petrova, Stefan Schulte-Merker, Mathias Francois, and Benjamin M. Hogan

SUPPLEMENTAL EXPERIMENTAL PROCEDURES. Related to main experimental procedures.

Additional animal procedures

For the induction of Cre-mediated recombination in embryos, 1.5 mg tamoxifen suspension in sunflower oil were injected intra-peritoneally into pregnant females at 9.5, 10.5 and 11.5 or 11.5, 12.5, 13.5 dpc in two separate regimes.

GOLPH4 processing - subtraction of background Golgi staining

The nucleus-Golgi angle relative to the dorsal midline was measured by first using the NRP2 expressing tissues as a mask to remove non-endothelial GOLPH4 staining during processing. The angle was subsequently measured between the perpendicular to the midline and the nucleus-Golgi orientation vectors in endothelial cells. Sphericity was measured in nuclei located within 150 μm of the leading edge, on both side of the midline in 14.5 dpc embryos. At earlier stages (10.5 and 11.5dpc), polarity and nuclear sphericity were assessed in cells at the lymphatic vascular migratory front only.

Statistical analysis

We used a Mann-Whitney rank sum t-test using Prism (GraphPad software), for all figures except in Figure 2 (**E**), Figure 4 (**G-H**) and Supplementary Figure 3 and 9 where a two-tailed unpaired Student's t test was used. P-values are represented in the Figures as *= $P \leq 0.05$, **= $P \leq 0.01$, ***= $P \leq 0.001$ and ****= $P \leq 0.0001$. Standard error of the mean is represented in error bars.

Whole-mount *in situ* hybridization and immunochemistry

Primers used to amplify templates for riboprobe production are presented below. All probe template cDNAs were amplified from stage mixed WT cDNA by PCR and all PCR products, except for *pkd1a*, were subsequently cloned into pCS2+ plasmid (Turner and Weintraub, 1994). *In situ* hybridization was performed essentially as described in (Habeck et al., 2002; Thisse et al., 1993), with NBT/BCIP staining solution (Roche). Expression analysis and plasmid probes for *flt4*, *dab2*, *couptfll*, *ephrinb2a*, *vegfc* probes has been previously described in (Aranguren et al., 2011; Hogan et al., 2009; Lawson et al.,

2001; Song et al., 2004; Thompson et al., 1998). Antibodies and primers used in this study are reported below.

Primers and antibody

The antibodies used in this study are: ENDOMUCIN (sc-53941, Santa Cruz Biotechnology, 1/200), NRP2 (AF567, R&D systems, 1/200), PROX1 (AF2727, R&D systems, 1/200), PROX1 (11-002, Angobio Co, 1/200), GOLPH-4 (ab28049, Abcam, 1/200), LYVE1 (Ab14917, Abcam, 1/200), LYVE1 (Ab14917, Abcam, 1/200), β -CATENIN (C2206, Sigma, 1/200), VE-CADHERIN (sc-6458, Santa Cruz Biotechnology, 1/200), Alexa fluor 647 (A21247, Invitrogen, 1/200), Alexa fluor 546 (A11010, Invitrogen, 1/200), Alexa Fluor 488 (A11055, Invitrogen, 1/200), Acetylated-tubulin (T7451, Sigma, 1/500). Primers used in this study are presented in Table 1.

Quantitative real time PCR analysis

Cell isolation, RNA extraction and cDNA synthesis: Zebrafish at 3 dpf and 5 dpf were deyolked by pipetting with 200 μ l pipette tip and rinsed in Calcium free ringers solution. Embryos were dissociated via treatment with 0.25% trypsin in PBS for early time points or a 1/35 dilution of liberase Tm (Roche) in PBS at 28°C with repeated pipetting. For the venous/lymphatic comparisons RNA was extracted from FACS sorted samples from 3 and 5 dpf *Tg(kdrl:GFP/lyve1:DsRed2)* zebrafish, with the DsRed/GFP positive cells corresponding to the venous cell population and the DsRed positive and GFP negative population corresponding to the lymphatic cell population. FACS analysis was performed at the Queensland Brain Institute (University of Queensland) using a Cytopeia Influx Cell Sorter (Cytopeia, Seattle USA). RNA extraction and genomic DNA removal was performed using a QIAGEN RNeasy micro kit (Qiagen Inc., Chatsworth, CA, USA) as per manufacturers recommendations. RNA was quantified using a NanoDrop 1000 spectrophotometer (Thermo Fisher Scientific, Waltham, MA, USA) and the integrity confirmed using an Agilent bioanalyser. RNA was amplified using the Agilent low input Quick Amp Labelling kit. For cDNA synthesis, residual genomic DNA was removed using the genomic DNA wipeout buffer included in the Quantitect reverse transcription kit (Qiagen Inc., Chatsworth, CA, USA). 30-50 ng of amplified mRNA was reverse transcribed into cDNA for 30 min at 42°C using a Quantitect reverse transcription kit (Qiagen Inc., Chatsworth, CA, USA) as per manufacturer's

recommendations. Specificity of the qPCR reactions was assessed in the absence of reverse transcriptase enzyme by including a no-transcript control (NTC).

Quantitative PCR: qPCR was performed using an Applied Biosystems Viia 7 384 well qPCR machine, Applied Biosystems). Each qPCR reaction mixture contained 7.5 μ l 2 x ABI SYBR green master mix (Applied Biosystems), 5ul cDNA (80-fold dilution), and 500 nM each primer to a final volume of 15 μ l. Amplification was performed in duplicate in 384 well plates (Applied Biosystems) with the following thermal cycling conditions: initial UDG treatment 50°C for 10 minutes, followed by 40 cycles of 15 s at 95°C, 60 s at 60°C. Control reactions included a no template control (NTC) and a no reverse transcriptase control (-RT). Dissociation analysis of the PCR products was performed by running a gradient from 60 to 95°C to confirm the presence of a single PCR product. The efficiency of PCR amplification was determined using LinReg PCR (Ruijter et al., 2009). The stability of several reference genes was analysed including *hprt1*, *ef1a*, *rps29*, *rpl13* and β -actin. Reference gene stability was determined using GeNorm (Vandesompele et al., 2002). The geometric average of *rps29*, *rpl13* and *ef1a* was used for normalisation of gene expression, except in Figure 2F where *rpl13* was used, these genes being validated as the most stable across the sample population.

Primer design: Primers were designed using Primer blast (<http://www.ncbi.nlm.nih.gov/tools/primer-blast/>) to have Tm of 60°C and to cross an exon-exon junction to avoid amplification of genomic DNA, whenever possible. Primers were used at a final concentration of 500 nM.

Human lymphatic endothelial cells

Human LECs were isolated and cultured as described (Norrmen et al., 2010). All experiments were performed with confluent cells.

PKD1 knockdown in human LECs

siRNA transfection

Human LECs were transfected with 50 nM of control siRNA (Qiagen, AllStars Negative Control siRNA) or *PKD1* siRNA (ThermoScientific, SmartPool containing 4 different siRNAs) using Lipofectamine RNAiMAX (Invitrogen).

shRNA transduction

Lentiviral particles were prepared using PLKO.1 lentivector (Sigma) either empty as a control or carrying shRNA against *PKD1*. Two different constructs were used, sh*PKD1*_a (TTGTAGACACAGAACTCCTCG) (Sigma, TRCN0000062320) and sh*PKD1*_b (AATGTCTTGCCAAAGACGGAC) (Sigma, TRCN0000062322). shRNA sequences do not overlap with siRNAs used in the transfection experiments. Lentiviral particles were quantified using p24 Elisa kit (Gentaur) according to manufacturer's instructions. Human LECs were transduced with a multiplicity of infection of 10. Three days post-transduction, cells were selected for two days in 300 ng/ml puromycin.

PKD1 knockdown validation

Total RNA was isolated using Qiagen RNeasy Plus Mini Kit (Qiagen) 24h post-transfection or 3 days post-transduction. Reverse transcription was performed using Transcriptor First Strand cDNA Synthesis Kit (Roche Diagnostics). Real-time qPCR analyses were performed on StepOnePlus (Applied Biosystems) using SYBR Green PCR Master Mix (Applied Biosystems). Sequences of PCR primers are included in table 1. Analysis of *PKD1* expression relative to *18s* was carried out using the comparative Ct ($\Delta\Delta C_t$) method as described by the manufacturer.

Lymphatic endothelial cell spheroid sprouting assay

800 LECs were seeded in round-bottom 96-well plates as described previously (Korff et al., 1999). The spheroids were collected and embedded in fibrin gels (2.5 mg/ml fibrinogen, 0.625 U/ml thrombin and 0.15 U/ml aprotinin), treated with 100 ng/ml BSA (Sigma) or $\Delta N\Delta C$ -VEGFC (kindly provided by Dr. M. Jeltsch and Dr. K. Alitalo) for 48 h. The spheroids were fixed in 4% PFA for 1 h at RT. Nuclei were stained with bis-Benzimide (Sigma) and F-actin cytoskeleton with Alexa 488-conjugated phalloidin (Molecular Probes). Spheroids (8 per condition) were imaged using Zeiss LSM 510 META scanning confocal microscope. The confocal images were processed using Bitplane IMARIS Suite 6.3.1 and Photoshop softwares. The number of sprouts, the cumulated length of sprouts, the average of sprout length and the density of nuclei composing the sprouts were measured for each spheroid using ImageJ

software. A two-tailed unpaired Student's t test was used to analyze the statistical significance of the difference between BSA- and VEGFC-treated, or Control and *PKD1*-knockdown groups.

Cell staining procedures and image acquisition

Cells cultured on coverlips were fixed with 4% PFA, permeabilized with 0.1% Triton X-100 and blocked with 5% donkey serum. We used Alexa 488-conjugated phalloidin (Molecular Probes), rabbit anti-human β -CATENIN (Upstate), goat anti-mouse VE-CADHERIN (R&D systems) and rabbit anti-human ZO-1 (Invitrogen). Coverslips were mounted using Prolong Gold anti-fade reagent containing Dapi (Invitrogen). Cells were imaged using Zeiss LSM 510 META scanning confocal microscope. The confocal images were processed using Bitplane IMARIS Suite 6.3.1 and Photoshop softwares.

Western blotting

Cells were lysed in a modified RIPA buffer, containing 50 mM Tris- HCl pH7.4, 0.25 mM Na-deoxycholate, 150 mM NaCl, 2 mM EGTA, 0.1 mM Na₃VO₄, 10 mM NaF, 1 mM PMSF, 1% Triton-X 100 and a complete protease inhibitor mixture (Roche). Protein concentration was measured using BCA kit (Pierce) and samples were resolved by SDS-PAGE, transferred onto Immobilon-P membrane (Millipore), and blotted with antibodies against rabbit anti-human GAPDH (Sigma), mouse anti-human β -CATENIN (BD transduction) and goat anti-mouse VE-CADHERIN (R&D systems). Western blots were developed using the ECL method (SuperSignal West Femto Maximum Sensitivity Substrate; Thermo Fisher Scientific).

Calcium drug treatment

Zebrafish embryos were exposed to DMSO, Nifedipine and Bayk8644 (Tocris Bioscience ref 1075 and 1544 respectively) at the concentration indicated in E3 media, from 24 hpf to 4 dpf. The treatment media was changed twice a day. Nifedipine and Bayk8644 were stored according to manufacturer recommendations.

SUPPLEMENTAL MOVIE LEGENDS

Supplemental Movie S1. Related to Figure 1.

Time-lapse visualization of PL (arrow) migration between 62 hpf and 92 hpf in the trunk of a WT embryo in *Tg(fli1a:EGFP; fli1:tomato)*. The video was acquired using a 10x objective, one frame every 20 minutes.

Supplemental Movie S2. Related to Figure 1.

Time-lapse visualization of PL (arrow) migration between 62hpf and 92hpf in the trunk of a *lyc1* embryo in *Tg(fli1a:EGFP; fli1:tomato)*. The video was acquired using a 10x objective, one frame every 20 minutes.

Supplemental Movie S3. Related to Figure 1.

Spinning disk visualization of a parachordal lymphangioblast between 56 and 64 hpf in the trunk of a control (WT/MO-*pkd1b*) embryo (5ng MO), which develop wildtype lymphatics. The video was acquired using a 40x dry objective, one frame every 4 minutes.

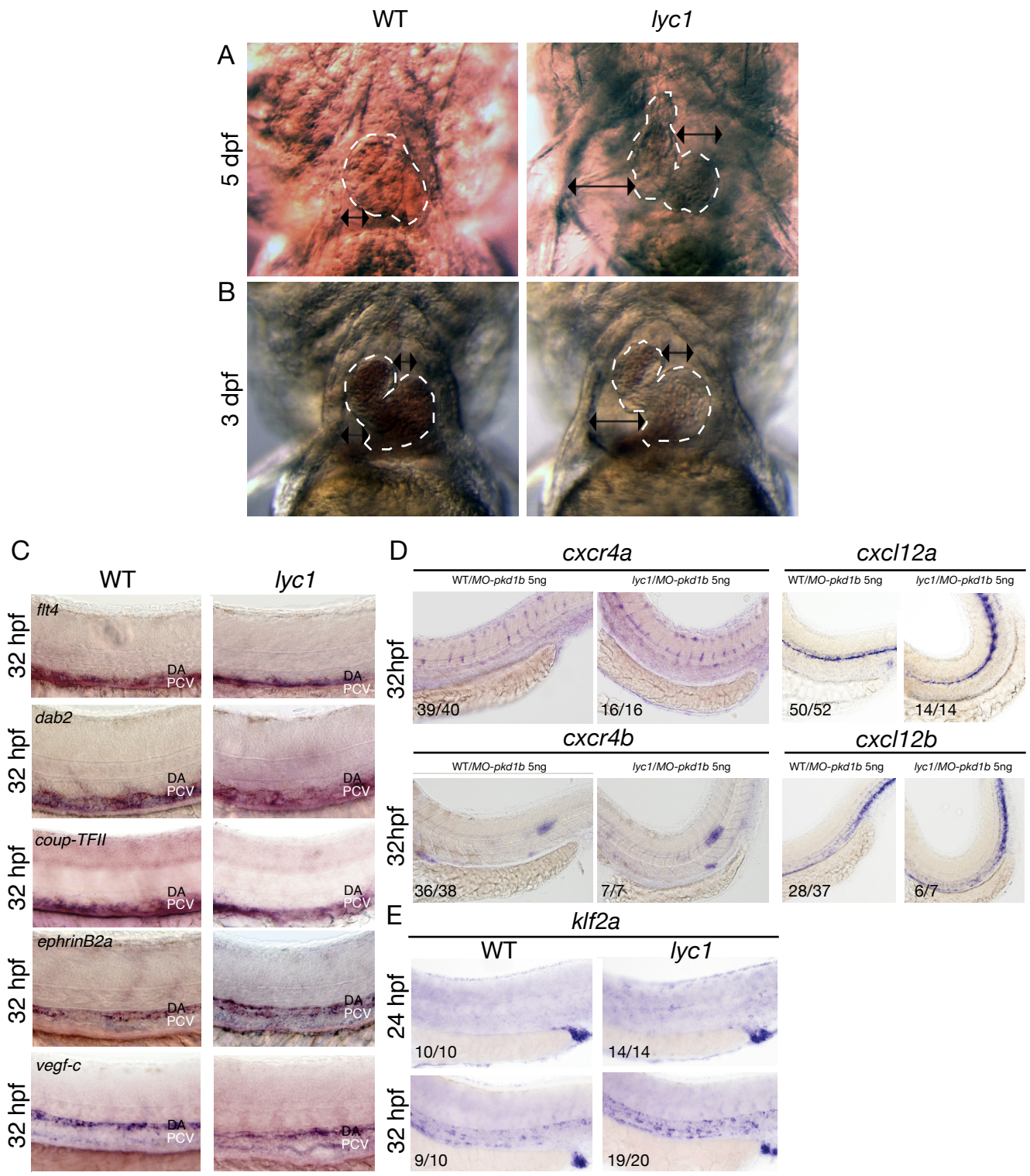
Supplemental Movie S4. Related to Figure 1.

Spinning disk visualization of a parachordal lymphangioblast between 56 and 64 hpf in the trunk of a *lyc1/MO-pkd1b* embryo (5ng MO). The video was acquired using a 40x dry objective, one frame every 4 minutes.

Supplemental Movie S5. Related to Figure S7.

Analysis of co-localisation of tdTOMATO with PROX1 and NRP2 during validation of the *Sox18:GFP-Cre-ERT2* using the *Cg-Gt(ROSA)26Sor^{tm9(CAG-tdTomato)Hze}/J* reporter strain. Computational masking of the area spanned by NRP2 expression using Imaris software allows for removal of the majority of blood vascular tdTOMATO. This identifies high activity of *Sox18:GCE* in LECs, allowing for counting of individual PROX1/tdTOMATO co-expressing LEC nuclei (CAG-tdTOMATO localizes strongly to nuclei) and revealing large clonal patches of CRE activity in subcutaneous lymphatic vessels.

Supplemental Figure 1



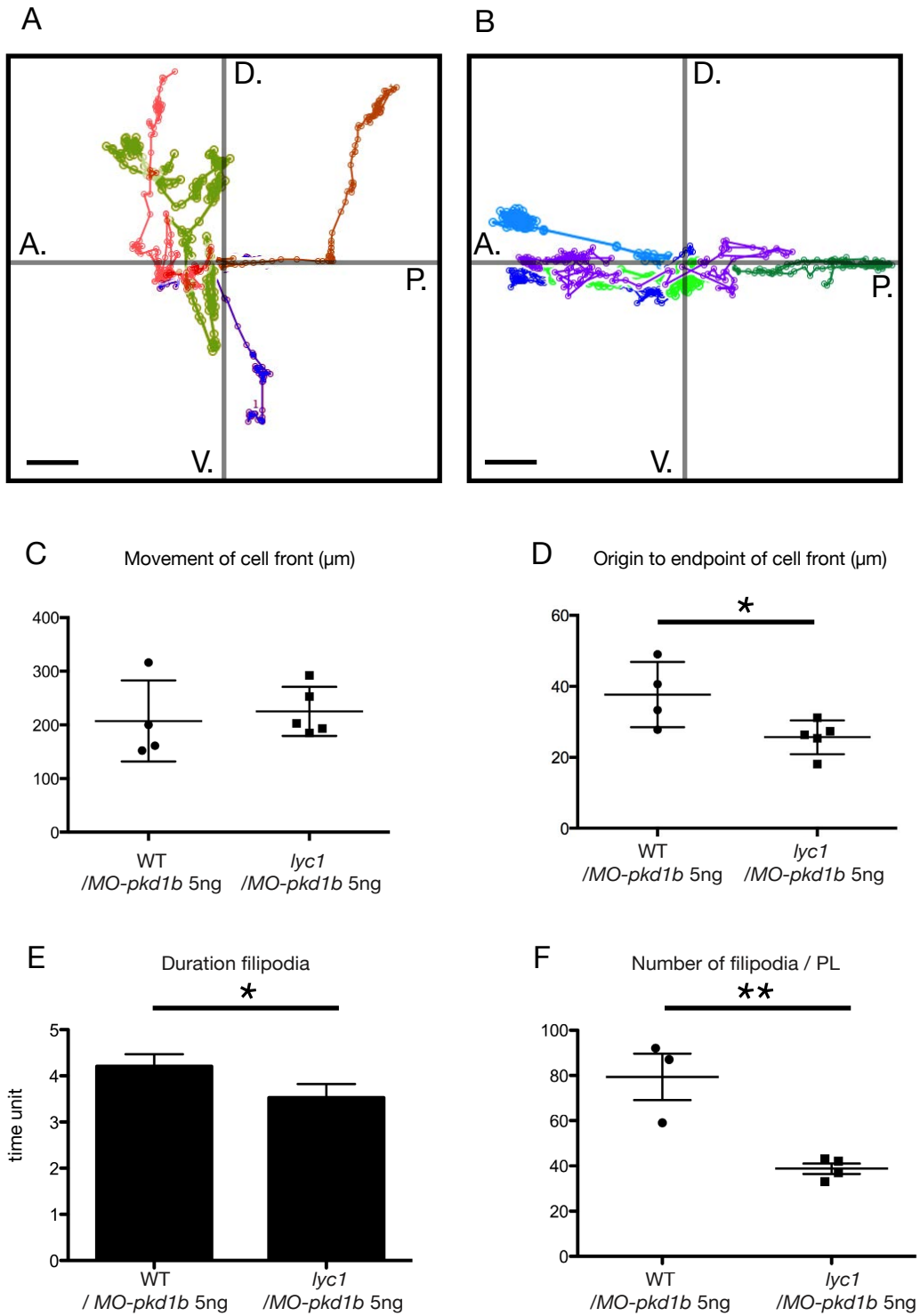
Supplemental Figure S1: Further phenotypic analysis of *lyc1*. Related to Figure 1

(A-B) Representative overall morphology of WT and *lyc1* mutant embryonic hearts and pericardial cavities at 3 (A) and 5 dpf (B). Double-sided arrows indicate the distance between the pericardium and heart. Dashed line indicates the outline of the myocardium.

(C) *In situ* hybridization analysis of *flt4* (n=22), *dab2* (n=16), *coup-TFII* (n=20), *ephrinb2a* (n=17) and *vegfc* (n=28) in *lyc1* mutant embryos revealed no alterations in normal expression patterns. N values indicate the total number of embryos examined from an incross of known heterozygotes (expected 25% *lyc1* mutants). Individual genotype confirmed mutant embryos are shown in the right hand panels. (D) Expression of *cxcr4a* was unchanged at 32 hpf in control WT/*MO-pkd1b* (embryos show no phenotype after *pkd1b* knockdown only and internally control for MO toxicity) (n=39/40) compared with phenotypically mutant (based on body curvature in the presence of *MO-pkd1b*) *lyc1/MO-pkd1b* embryos (5ng MO) (n=16/16). Expression of *cxcr4b* was unchanged at 32 hpf in control (WT/*MO-pkd1b*) (n=36/38) compared with phenotypically mutant *lyc1/MO-pkd1b* embryos (5ng MO) (n=7/7). Expression of *cxcl12a* was unchanged at 32 hpf in control (WT/*MO-pkd1b*) (n=50/52) compared with phenotypically mutant *lyc1/MO-pkd1b* embryos (5ng MO) (n=14/14). Expression of *cxcl12b* was unchanged at 32 hpf in control (WT/*MO-pkd1b*) (n=28/37) compared with phenotypically mutant *lyc1/MO-pkd1b* embryos (5ng MO) (n=6/7).

(E) Expression of *klf2a* at 24 (n=10/10) and 32 hpf (n=9/10) is normal in WT embryos. Expression of *klf2a* at 24 hpf (n=14/14) and 32 hpf (n=19/20) in *lyc1* mutant embryos.

Supplemental Figure 2



Supplemental Figure S2: Parachordal lymphangioblasts fail to directionally migrate and display altered cell dynamics in the *lyc1* mutant. Related to Figure 1.

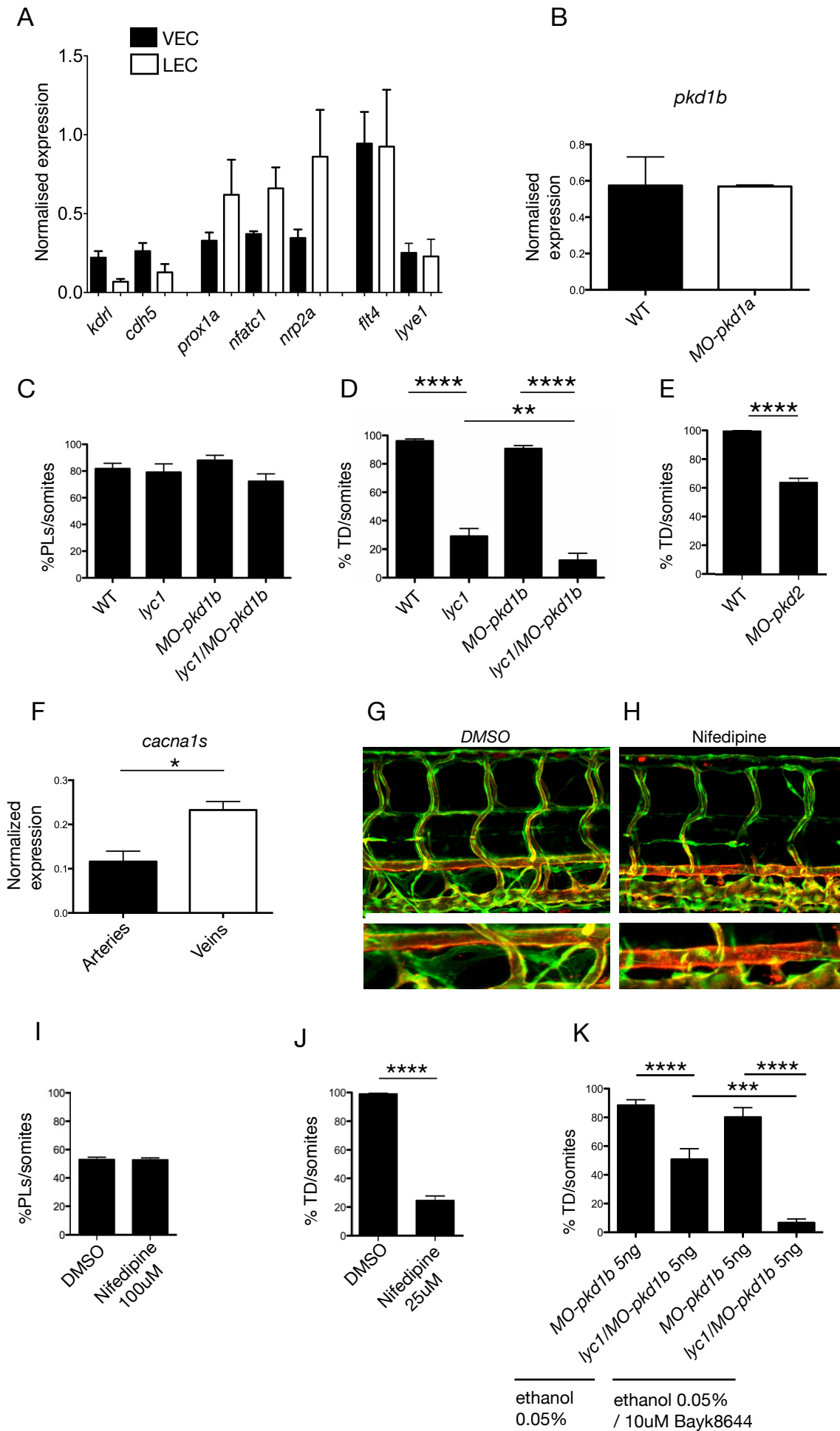
(A-B) Schematic overview of the movement of the leading front of individual parachordal lymphangioblasts (t=10.5h) from 56 hpf (scale bar: 10 μ m) in **(A)** WT/*MO-pkd1b* (5ng MO) (n=3 embryos, n=4 leading fronts) and **(B)** phenotypically mutant *lyc1/ MO-pkd1b* (5ng MO) (n=5 embryos, n=5 leading fronts).

(C-D) Quantification of **(C)** movement of cell front and **(D)** origin to endpoint of cell front distance migrated by parachordal lymphangioblasts (t=10.5h) from 56 hpf in WT/*MO-pkd1b* (5ng MO) (n=3 embryos, n=4 leading front) and phenotypically mutant *lyc1/ MO-pkd1b* (5ng MO) (n=5 embryos, n=5 leading fronts) (μ m).

(E) Quantification of duration of individual filipodial extensions in single parachordal lymphangioblasts at the horizontal myoseptum by time-lapse imaging (spinning disc). WT/*MO-pkd1b* (n=3) and phenotypically mutant *lyc1/ MO-pkd1b* embryos (n=4) (5ng MO) were examined between 56-64 hpf (1 time unit = 4 minutes).

(F) Quantification of the number of filipodial extensions per parachordal lymphangioblasts by time-lapse imaging (spinning disc) in WT/*MO-pkd1b* (n=3) and phenotypically mutant *lyc1/ MO-pkd1b* embryos (n=4) (5ng MO) between 56-64 hpf.

Supplemental Figure 3



Supplemental Figure S3: The *lyc1* mutant lymphatic phenotype is enhanced with *MO-pkd1b* injection and targeting calcium signaling results in a lymphatic phenotype. Related to Figure 2.

(A) Quantitative real time PCR for *kdr1*, *cdh5*, *prox1a*, *nfatc1*, *nrp2a*, *flt4* and *lyve1* transcripts normalized expression at 3 dpf in sorted embryonic venous and lymphatic endothelial cells. Sorted cell populations display the predicted enrichment of marker genes.

(B) Quantitative real time PCR for *pkd1b* transcript normalized expression against *ef1a* and *rpl13* at 3 dpf in WT and *MO-pkd1a* embryos at 24hpf. *pkd1b* is readily detectable in whole embryo cDNA but not altered by *pkd1a* knockdown.

(C) Quantification of parachordal lymphangioblasts in WT (n=18), *lyc1* (n=9) WT/*pkd1b* (5ng MO) (n=21), *lyc1/MO-pkd1b* embryos (5ng MO) (n=23) at 56hpf.

(D-E) Quantification of thoracic duct extent in **(D)** WT (n=48), *lyc1* (n=23), WT/*MO-pkd1b* (5ng MO) (n=24), *lyc1/MO-pkd1b* embryos (5 ng MO) (n=21), and **(E)** WT (n=50), *MO-pkd2* embryos (7.5 ng MO)(n=136) at 4dpf.

(F) Quantitative real time PCR for *cacna1s* transcript normalized expression at 30 hpf in sorted embryonic venous and arterial endothelial cells. Endothelial expression of this calcium channel and Nifedipine target is confirmed.

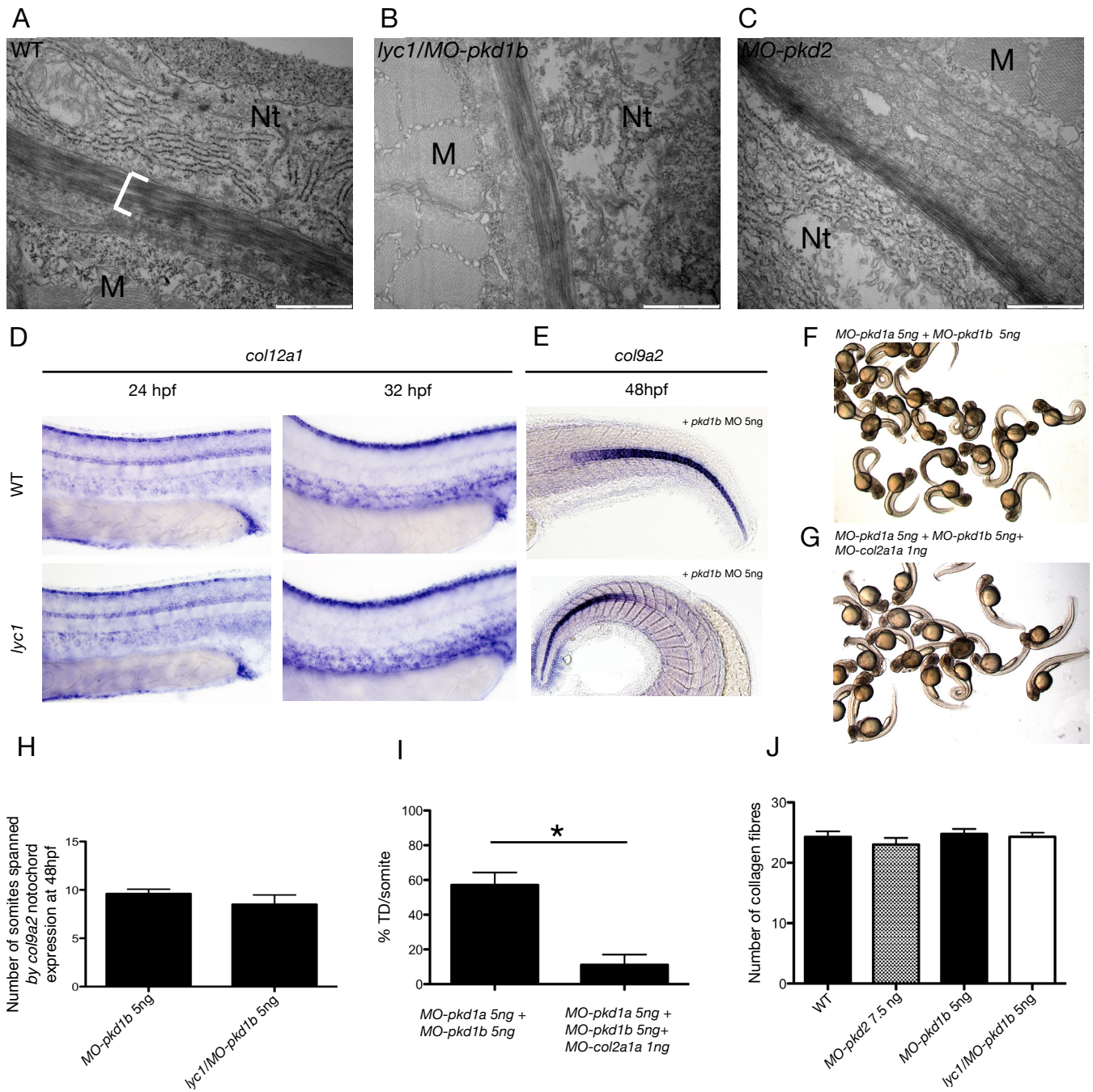
(G-H) The vasculature of **(G)** DMSO 0.05% and **(H)** DMSO 0.05%/Nifedipine 25 μ M treated embryos in Tg(*fli1a:EGFP^{y1}*; *kdr1:mcherry^{s916}*). The thoracic duct is markedly absent in the presence of a calcium signaling antagonist (Nifedipine).

(I) Quantification of parachordal lymphangioblasts in DMSO 0.2% (n=62) and DMSO 0.2%/Nifedipine 100 μ m treated embryos (n=101) at 56 hpf. PLs are unchanged in the presence of a calcium signaling antagonist (Nifedipine).

(J) Thoracic duct quantification in DMSO 0.05% (n=45) and DMSO/0.05%/Nifedipine 25 μ M (n=68) at 5 dpf. Thoracic duct reduction similar to *lyc1* mutants is observed.

(K) Quantification of thoracic duct extent in WT/*MO-pkd1b*/0.05% ethanol (5ng MO) (n=21), *lyc1/MO-pkd1b*/0.05% ethanol (5ng MO) (n=21), *MO-pkd1b*/ethanol 0.05%/Bayk8644 (5ng MO) (n=28) and *lyc1/MO-pkd1b* /ethanol 0.05%/Bayk8644 (5ng MO)(n=15) embryos at 4dpf. A mildly penetrant *lyc1* carrier was used. Remarkably, a phenotypic interaction with the calcium agonist is observed only in the mutant animals and not in the wildtype siblings. This suggests a sensitivity of mutant cells to further fluctuations in Ca²⁺ signaling.

Supplemental Figure 4



Supplemental Figure S4: The *lyc1* lymphatic vascular phenotype is independent of collagen gene expression and ECM changes. Related to Figure 2.

(A-C) Electron-microscopy imaging of the peri-notochordal region in WT, *lyc1/MO-pkd1b* (5ng MO) and *MO-pkd2* embryos (7.5 ng MO). Nt=notochord, M=muscle.

(D) Expression of *col12a1*, a vascular collagen, was unchanged at 24 and 32 hpf in control (WT/*MO-pkd1b*) (n=27, n=37 respectively) compared with phenotypically mutant *lyc1/MO-pkd1b* embryos (5ng MO) (n=37, n=12 respectively).

(E) Expression of *col9a2* was unchanged at 48 hpf in control (WT/*MO-pkd1b*) (n=10) compared with phenotypically mutant *lyc1/MO-pkd1b* embryos (5ng MO) (n=10).

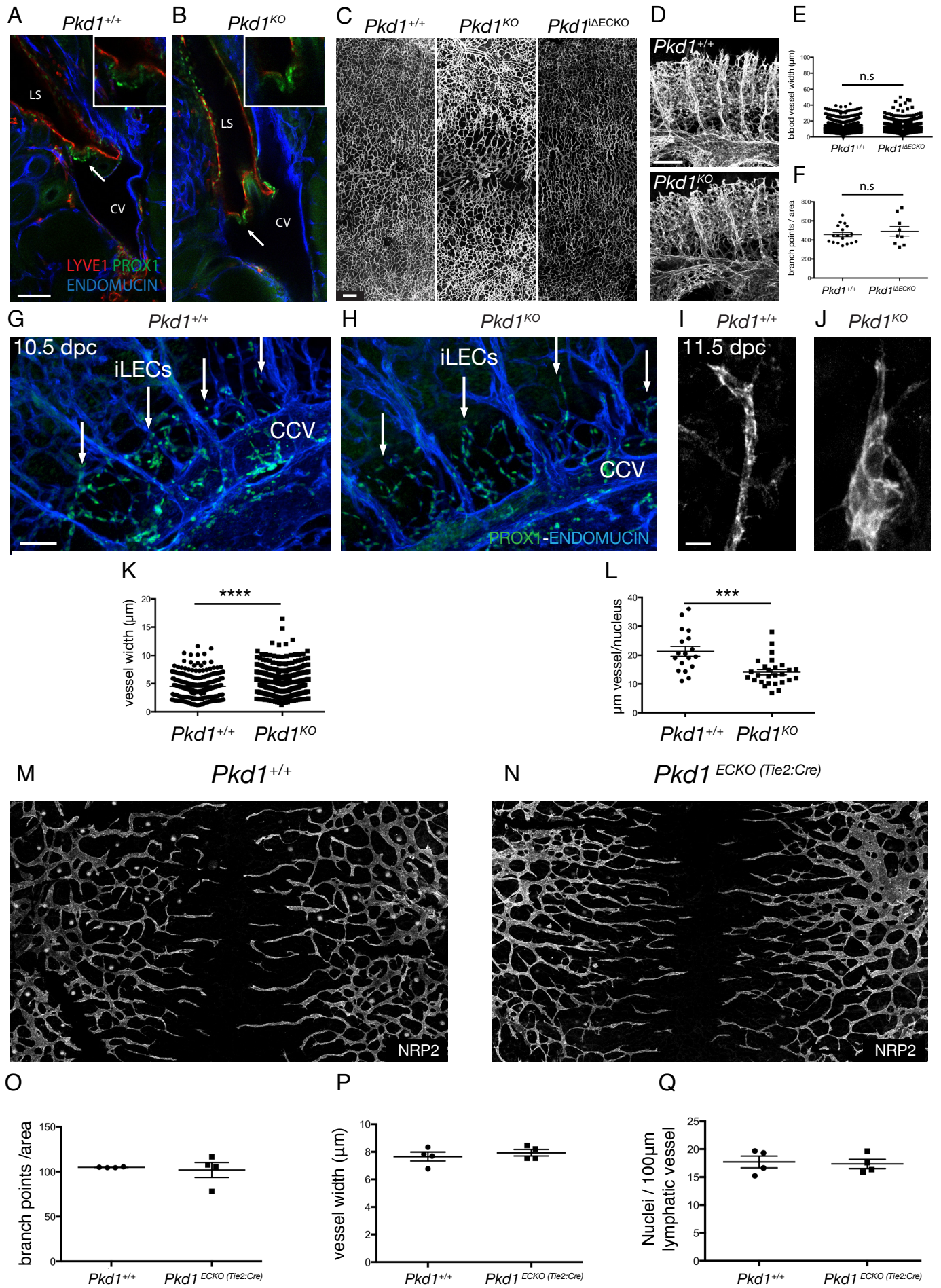
(F-G) Overall morphology of **(F)** *MO-pkd1a/MO-pkd1b* (5ng MO each) and **(G)** *MO-pkd1a/MO-pkd1b/MO-col2a1a* morphants (5,5,1 ng MO respectively). Knockdown of *Col2a1a* rescues the gross curvature phenotype as previously described (Mangos et al., 2010).

(H). Quantification of *col9a2* expression as the anterior posterior extent of expression in the notochord, delineated by somites boundaries. No increase in *col9a2* extent was observed.

(I) Quantification of thoracic duct extent in *MO-pkd1a/MO-pkd1b* embryos (n=21) and *pkd1a/pkd1b/col2a1a* morphants (n=19). Despite rescue of the gross curvature phenotype, TD extent is not rescued.

(J) Quantification of the number of collagen fibers in the medial layer of the peri-notochordal region in WT (n=3), WT/*MO-pkd2* (7.5 ng MO) (n=3), WT/*MO-pkd1b* (5 ng MO) (n=3) and *lyc1/MO-pkd1b* embryos (5ng MO)(n=3). No change was observed in peri-notochordal collagen.

Supplemental Figure 5



Supplemental Figure S5: Endothelial knockout of *Pkd1* does not affect blood vascular development and lymphatic morphological defects are observed in *Pkd1*^{KO} embryos from 11.5 dpc. Related to Figure 3.

(A-B) Overall morphology of lymphovenous valves in (A) WT (n=2) and (B) *Pkd1*^{KO} (n=3) coronal sections stained with PROX1, LYVE1 and ENDOMUCIN based on previous studies (Srinivasan and Oliver, 2011). **LS**: Lymph sac; **CV**: Cardinal Vein. White arrow and inset indicate lymphovenous valve. Scale bar: 100 μ m

(C) Representative morphology of subcutaneous blood vascular network in WT (n=7), *Pkd1*^{KO} (n=7), *Pkd1*^{i Δ ECKO} (n=3) at 14.5 dpc, stained with ENDOMUCIN. Scale bar: 200 μ m

(D) Lateral views of the representative morphology of the blood vascular network in whole mount WT (n=5) and *Pkd1*^{KO} (n=5) embryos at 11.5 dpc, stained with ENDOMUCIN. Scale bar: 100 μ m

(E) Quantification of the width of subcutaneous vessels (μ m) across the whole skin in WT (n=6), and *Pkd1*^{i Δ ECKO} (n=3) embryos (n=2398, n=1200 measurements respectively. Two areas of 2000*900 μ m centered on the midline were used for quantification in every embryo).

(F) Quantification of the number of branch points per area in WT (n=6) and *Pkd1*^{i Δ ECKO} (n=3) embryos (3 areas of 2000*500 μ m centered on the midline were used for quantification in every embryo).

(G,H) Representative lateral view of (G) WT (n=5) and (H) *Pkd1*^{KO} (n=5) bisected embryos with at 10.5 dpc stained with ENDOMUCIN and PROX1. Scale bar: 50 μ m. CCV: common cardinal vein, iLECs: initial lymphatic endothelial cells.

(I,J) Morphology of representative sLECs in (I) WT (n=5) and (J) *Pkd1*^{KO} (n=5) embryos stained for NEUROFILIN2. Scale bar: 10 μ m

(K) Quantification of the average width of leading sprouts (μ m) in WT (n=5) and *Pkd1*^{KO} (n=5), (n=18, n=27 measurements respectively, across leading lymphatic vessels, averaged) at 11.5 dpc.

(L) Quantification of nuclei per μ m of vessel in WT (n=5) and *Pkd1*^{KO} (n=5) (n=39, n=66 measurements respectively) at 11.5dpc.

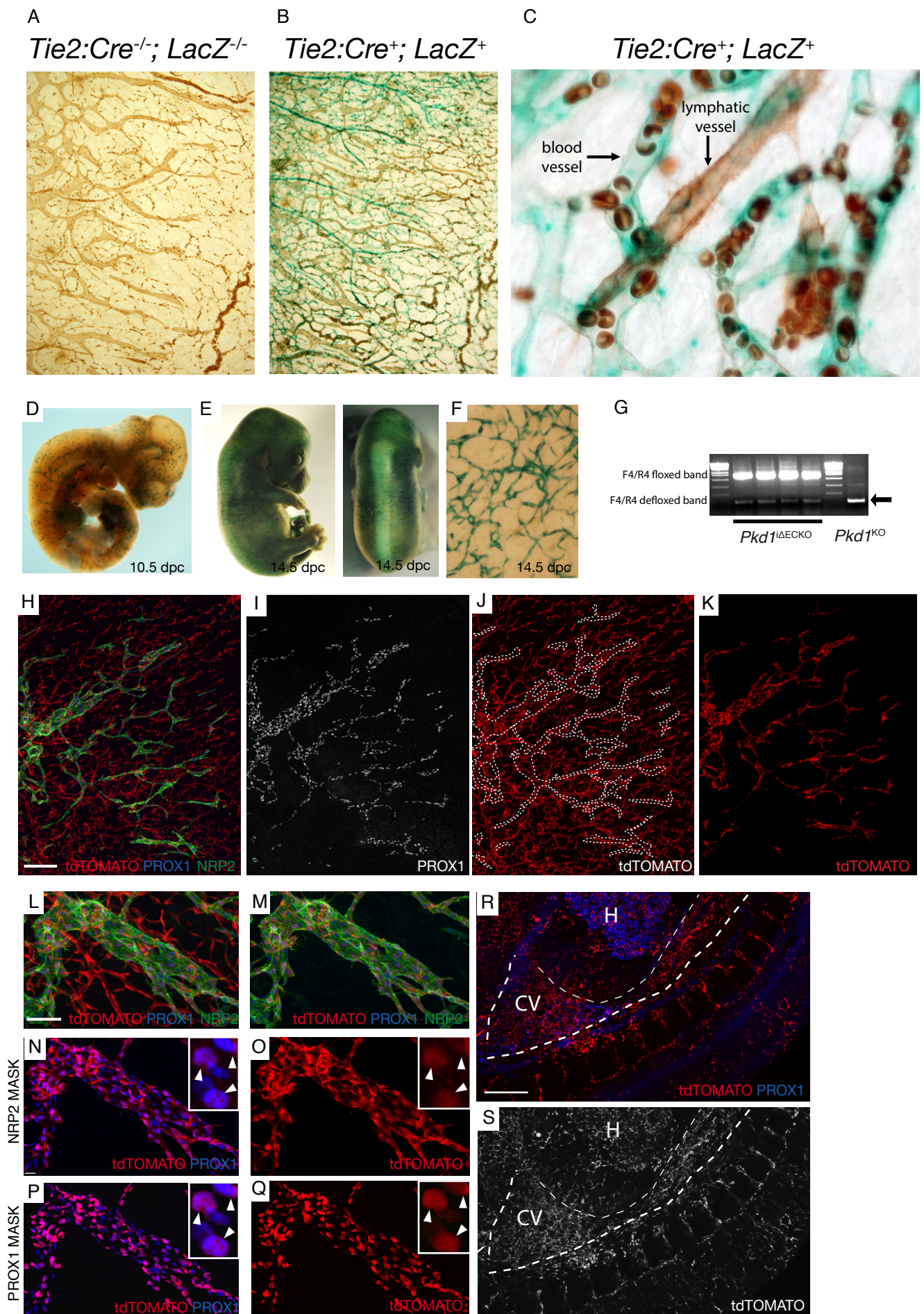
(M-N) Subcutaneous lymphatic vasculature in WT and *Pkd1*^{ECKO} (*Tie2:Cre+*; *Pkd1*^{ff}) mutants at 14.5 dpc.

(O) Quantification of branch points/area (2000*1500 μ m area on both sides of the midline) in WT (n=4 embryos) and *Pkd1*^{ECKO} (*Tie2:Cre+*; *Pkd1*^{ff}) (n=4 embryos) embryos at 14.5 dpc.

(P) Quantification of the average width of lymphatic vessels (μm) across the whole skin in WT (n=4 embryos) and *Pkd1*^{ECKO} (*Tie2:Cre+*; *Pkd1*^{ff}) (n=4 embryos) embryos. The average is shown of n=800 and n=800 measurements respectively, across leading lymphatic vessels from both side of the midline at 14.5 dpc.

(Q) Quantification of nuclei/100 μm length of vessel in WT (n=4 embryos) and *Pkd1*^{ECKO} (*Tie2:Cre+*; *Pkd1*^{ff}) (n=4 embryos) (n=10 representative vessels were counted per embryo at the leading edge and averaged) at 14.5 dpc.

Supplemental Figure 6



Supplemental Figure S6: Validation of gene targeting. Related to Figure 3.

(A-C) Whole mount X-gal staining of β -gal in *Tie2:Cre^{-/-}, Rosa26R^{-/-}* and *Tie2:Cre⁺, Rosa26R⁺* embryos shows that the Cre activity in the subcutaneous vasculature is strong in the blood vascular endothelium but not the lymphatic vascular endothelium at 14.5 dpc.

(D-E) Whole mount X-gal staining of β -gal in *Sox18-CREert2, Rosa26R* embryos show CREert2 activity in 10.5 and 14.5 dpc embryos.

(F). Whole mount X-gal staining indicates CRE activity, which is selective for endothelial cells, recapitulating the *Sox18* expression pattern. Note that there is no co-stain to determine vessel identity in this experiment.

(G) Genotyping of *Pkd1* ^{Δ ECKO} with primers F4/R4 (Piontek et al., 2004) shows a band indicating a defloxing event (subsequently confirmed by sequencing). This shows that the *Pkd1* locus is inactivated in a proportion of cells in the endothelial specific *Sox18:GCE* strain (DNA from whole tissue extract).

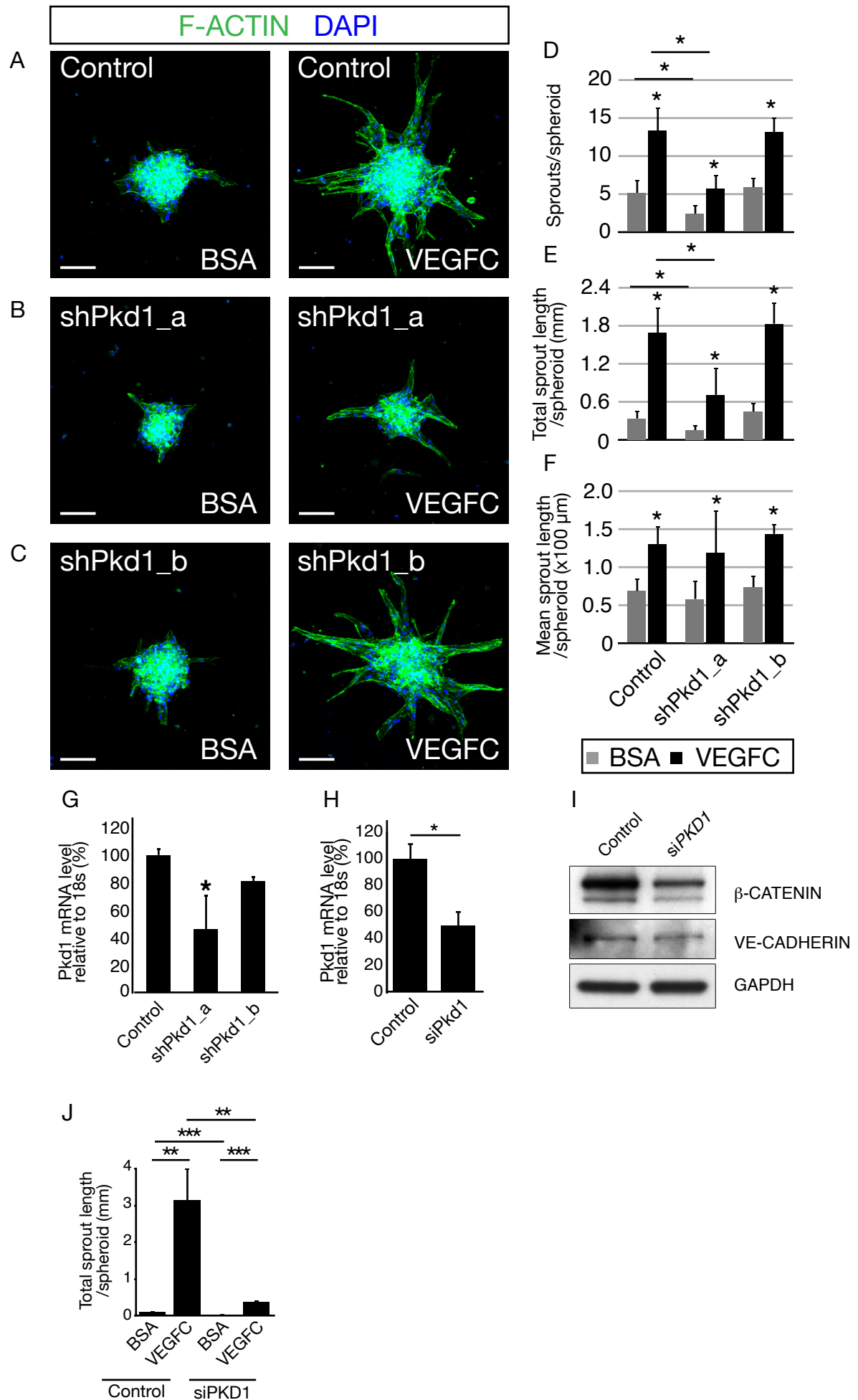
(H-K) Subcutaneous vessels analysed in *Sox18:GFP-Cre-ERT2, Cg-Gt(ROSA)26Sor^{tm9(CAG-tdTomato)Hze/J}* co-stained with NRP2 and PROX1 to identify the lymphatic vessels at 13.5 dpc. **H**. Low magnification image of whole skin showing tdTOMATO expression in blood and lymphatic endothelial cells. **I**. PROX1 stains only the lymphatic vessels. **J**. Lymphatic vessels make up a proportion of total cells expressing tdTOMATO (indicated by the hashed lines). **K**. Image processing to remove most blood vascular tdTOMATO (by computational masking of NRP2 positive tissue using Imaris software) reveals strong activity of *Sox18:GFP-Cre-ERT2* in cells of the lymphatic network. Scale bar: 200 μ m

(L-O). Example of a lymphatic vessel with tdTOMATO expression as analysed by Imaris image processing to remove non-lymphatic endothelial staining (eg, panels **M-O**). Inset in **N** and **O** are individual co-stained nuclei (PROX1 and tdTOMATO (CAG-tdTOMATO localizes to nuclei)) allowing precise cell counting. Quantification of whole skin as described in Figure 3 and related text, using this approach revealed that n=663/1138 LECs were tdTOMATO, PROX1 and NRP2 positive (58.2%).

(P-Q) Alternative masking in Imaris using PROX1 expression as the mask identified the same co-localisation as using an NRP2 mask (inset are individual nuclei). Scale bar: 10 μ m

(R-S) *Sox18:GFP-Cre-ERT2, Cg-Gt(ROSA)26Sor^{tm9(CAG-tdTomato)Hze/J}* co-stained with LYVE1 and PROX1 at 11.5 dpc labels the cardinal vein from which early LECs derive. CV: Cardinal Vein, H: Heart. Scale bar: 300 μ m

Supplemental Figure 7



Supplemental Figure S7: Validation of shRNA and siRNA targeting of *PKD1* expression in LECs *in vitro*. Related to Figure 4.

(A-C) Morphology of human LEC spheroids treated with control and two alternative *PKD1* shRNA (sh*Pkd1_a* and sh*Pkd1_b* respectively) in BSA or VEGFC supplemented conditions, stained with F-ACTIN (green) and DAPI (blue). Scale bar: 100 μ m.

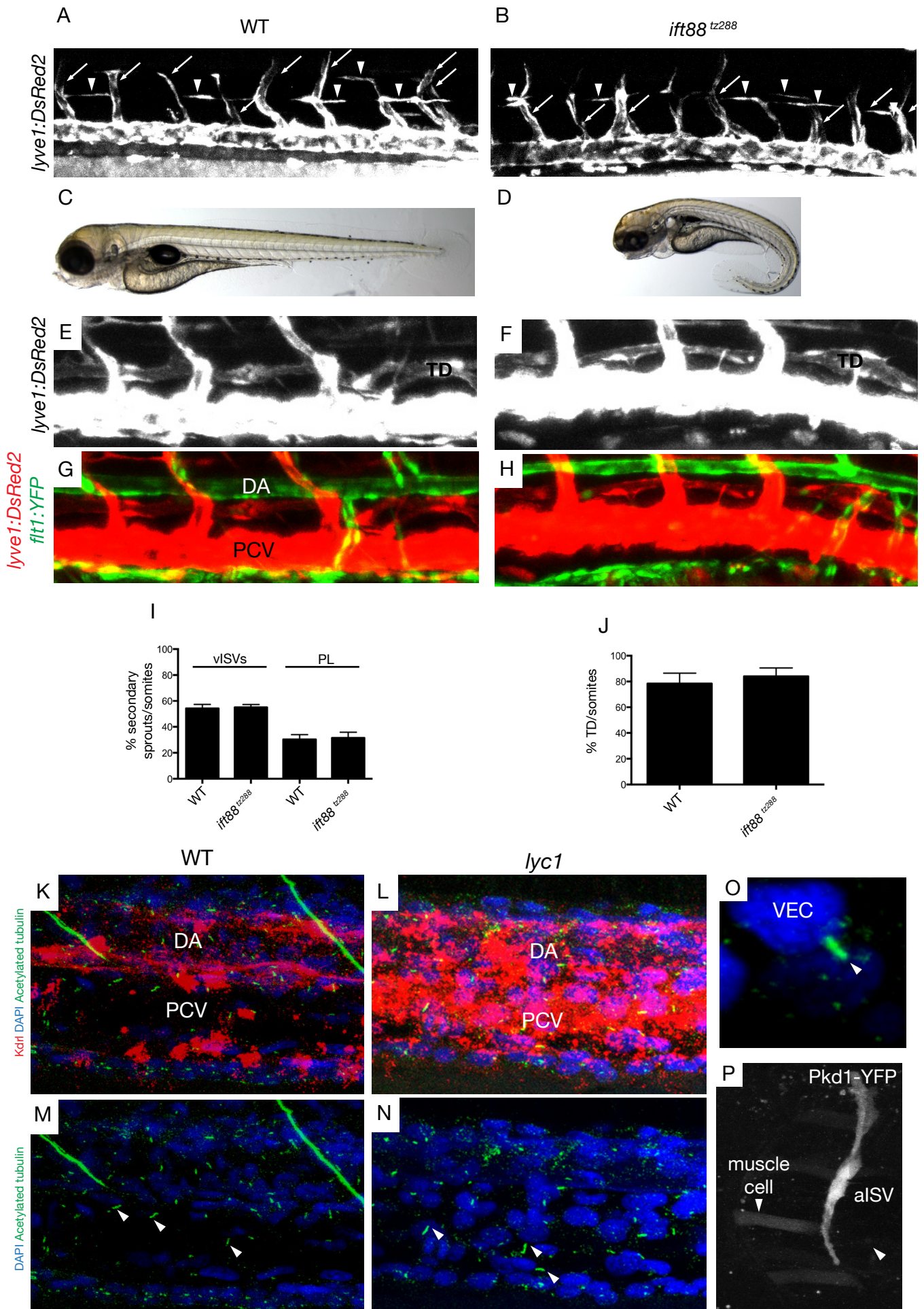
(D-F) Quantification of number of sprouts (**D**), total sprout length (mm) (**E**) and number of nuclei per 100 μ m of sprouts (**F**) in spheroids treated with control or *PKD1* targeting shRNA (sh*Pkd1_a* and sh*Pkd1_b* respectively) in BSA or VEGFC supplemented conditions.

(G-H) Quantification of *PKD1* mRNA expression level relative to 18s in human LEC spheroids treated with control and two alternative *PKD1* shRNA (sh*Pkd1_a* and sh*Pkd1_b* respectively) (**G**) and with control and *PKD1* targeting siRNA (**H**) in VEGFC supplemented conditions.

(I) Western-blot quantification of β -CATENIN, VE-CADHERIN and GAPDH protein levels in cultured human LECs treated with control and *PKD1* targeting siRNA.

(J) Quantification of total sprout length (mm) in spheroid treated with control or *PKD1* targeting siRNA in BSA or VEGFC supplemented conditions.

Supplemental Figure 8



Supplemental Figure S8: No evidence for a contribution of primary cilia to lymphangiogenesis.

Related to Discussion section.

(A-B) The vasculature Tg(*lyve1:DsRed2*)^{nz101} in (A) wild-type sibling and (B) *ift88*^{tz288} mutant embryos at 56 hpf (arrowheads indicate parachordal lymphangioblasts and white arrows indicate venous sprouts).

(C-D) Overall morphology of (C) wild-type siblings and (D) *ift88*^{tz288} mutants at 5 dpf. (E-H) The vasculature Tg(*lyve1:DsRed2*)^{nz101}; *flt1:YFP*^{hu4624Tg} of (E,G) WT and (F,H) *ift88*^{tz288} mutants at 5 dpf.

(I-J) Quantification of (I) secondary sprouts in WT (n=12) and *ift88*^{tz288} (n=10) at 56 hpf and (J) thoracic duct extent in WT (n=16) and *ift88*^{tz288} (n=18).

(K-N) Overview of primary cilia localization in the trunk of (K,M) WT (n=4) and (L,N) *lyc1* mutants (n=3) embryos at 30 hpf, stained for blood vessels (Kdrl-Cherry), nuclei (DAPI) and primary cilia (Acetylated-tubulin) markers. Arrowheads indicate example of discrete primary cilia.

(O) An individual representative primary cilium in a *lyc1* embryo.

(P) Transient expression of a Pkd1-YFP BAC construct in an arterial intersegmental vessel and adjacent muscle cells at 4 dpf. **DA**: Dorsal Aorta, **PCV**: Posterior Cardinal Vein, **TD**: Thoracic duct

Supplemental References

Aranguren, X.L., Beerens, M., Vandeveld, W., Dewerchin, M., Carmeliet, P., and Lutun, A. (2011). Transcription factor COUP-TFII is indispensable for venous and lymphatic development in zebrafish and *Xenopus laevis*. *Biochem Biophys Res Commun* *410*, 121-126.

Habeck, H., Odenthal, J., Walderich, B., Maischein, H., Schulte-Merker, S., and Tubingen screen, c. (2002). Analysis of a zebrafish VEGF receptor mutant reveals specific disruption of angiogenesis. *Curr Biol* *12*, 1405-1412.

Hogan, B., Bos, F., Bussmann, J., Witte, M., Chi, N., Duckers, H., and Schulte-Merker, S. (2009). *Ccbe1* is required for embryonic lymphangiogenesis and venous sprouting. *Nature genetics* *41*, 396-398.

Lawson, N.D., Scheer, N., Pham, V.N., Kim, C.H., Chitnis, A.B., Campos-Ortega, J.A., and Weinstein, B.M. (2001). Notch signaling is required for arterial-venous differentiation during embryonic vascular development. *Development* *128*, 3675-3683.

Mangos, S., Lam, P., Zhao, A., Liu, Y., Mudumana, S., Vasilyev, A., Liu, A., and Drummond, I. (2010). The ADPKD genes *pkd1a/b* and *pkd2* regulate extracellular matrix formation. *Dis Model Mech* *3*, 354-365.

Norrmen, C., Vandeveld, W., Ny, A., Saharinen, P., Gentile, M., Haraldsen, G., Puolakkainen, P., Lukanidin, E., Dewerchin, M., Alitalo, K., *et al.* (2010). Liprin (beta)1 is highly expressed in lymphatic vasculature and is important for lymphatic vessel integrity. *Blood* *115*, 906-909.

Piontek, K.B., Huso, D.L., Grinberg, A., Liu, L., Bedja, D., Zhao, H., Gabrielson, K., Qian, F., Mei, C., Westphal, H., *et al.* (2004). A functional floxed allele of *Pkd1* that can be conditionally inactivated in vivo. *Journal of the American Society of Nephrology : JASN* *15*, 3035-3043.

Ruijter, J.M., Ramakers, C., Hoogaars, W.M., Karlen, Y., Bakker, O., van den Hoff, M.J., and Moorman, A.F. (2009). Amplification efficiency: linking baseline and bias in the analysis of quantitative PCR data. *Nucleic Acids Res* *37*, e45.

Song, H.D., Sun, X.J., Deng, M., Zhang, G.W., Zhou, Y., Wu, X.Y., Sheng, Y., Chen, Y., Ruan, Z., Jiang, C.L., *et al.* (2004). Hematopoietic gene expression profile in zebrafish kidney marrow. *Proc Natl Acad Sci U S A* *101*, 16240-16245.

Srinivasan, R.S., and Oliver, G. (2011). *Prox1* dosage controls the number of lymphatic endothelial cell progenitors and the formation of the lymphovenous valves. *Genes & development* *25*, 2187-2197.

Thisse, C., Thisse, B., Schilling, T.F., and Postlethwait, J.H. (1993). Structure of the zebrafish *snail1* gene and its expression in wild-type, spadetail and no tail mutant embryos. *Development* *119*, 1203-1215.

Thompson, M.A., Ransom, D.G., Pratt, S.J., MacLennan, H., Kieran, M.W., Detrich, H.W., 3rd, Vail, B., Huber, T.L., Paw, B., Brownlie, A.J., *et al.* (1998). The *cloche* and *spadetail* genes differentially affect hematopoiesis and vasculogenesis. *Dev Biol* *197*, 248-269.

Turner, D.L., and Weintraub, H. (1994). Expression of *achaete-scute* homolog 3 in *Xenopus* embryos converts ectodermal cells to a neural fate. *Genes Dev* *8*, 1434-1447.

Vandesompele, J., De Preter, K., Pattyn, F., Poppe, B., Van Roy, N., De Paepe, A., and Speleman, F. (2002). Accurate normalization of real-time quantitative RT-PCR data by geometric averaging of multiple internal control genes. *Genome biology* 3, RESEARCH0034.

Table 1 Primers used in this study

Name	Use	Sequence direction	Sequence
marker 1 - 54.65Mb	polymorphic marker used for positional cloning	F	5'-GACTACACCGGTTGTGTCTG-3'
		R	5'-GTCCCTTCAGATCGGTCAC-3'
marker 2 - 54.73Mb	polymorphic marker used for positional cloning	F	5'-ACCACACAGACAAACTCTGG-3'
		R	5'-CGTCACATGTTGATCACAGAC-3'
marker 3 - 54.77Mb	polymorphic marker used for positional cloning	F	5'-CAGAGGCTTCTCCTATCACAC-3'
		R	5'-TGACAACCATGCTTTGAGTC-3'
marker 4 - 54.92Mb	polymorphic marker used for positional cloning	F	5'-TGAACAAATGGTCGCATGTT-3'
		R	5'-ACTTTTCCATCTGCTGCTCC-3'
<i>lyc1</i> mutation site	sequencing <i>lyc1</i> mutation (R3607X)	F	5'-TTGCTATTCTGTGTGTTCTG-3'
		R	5'-ACATCAACCGTCTGACATC-3'
<i>lyc1</i> mutation site	Introduction of an Hinp11 restriction fragment length polymorphism by PCR for rapid genotyping of <i>lyc1</i> fish. The presence of the <i>lyc1</i> stop codon mutation in the <i>pkd1a</i> sequence removes the induced Hinp11 restriction cutting site.	Hinp11-R	5'CGCACTCGGGGATCCGCTGGACCACGC-3'
<i>pkd1a</i> riboprobe	riboprobe amplification with T3 polymerase Tag	F	5'-ACGTGTGTGTCTCTGGAC-3'
		R	5'GGATCCATTAACCCCTCACTAAAGGGAAGTACTCTGGTATTGTGTGC-3'
<i>cxcl12a</i> cloning	subcloning riboprobe in PCS2+ vector	F	5'-GCGCGAATTCAAAAAGCCCAACAGCAGCAGG-3'
	[restriction sites in bold]	R	5'-GCGCCTCGAGACACGGAGCAAACAGGACTCC-3'
<i>cxcl12b</i> cloning	subcloning riboprobe in PCS2+ vector	F	5'-GCGCGAATTCATTGCCAGCAATGTTTCGC-3'
	[restriction sites in bold]	R	5'-GCGCCTCGAGTGTGACCAGAGGGCTAGTGT-3'
<i>cxcr4a</i> cloning	subcloning riboprobe in PCS2+ vector	F	5'-GCGCGAATTCGTCTCACTCTGCCATTCTGG-3'
	[restriction sites in bold]	R	5'-GCGCCTCGAGACAGCAGTGAAAGTACGCGA-3'
<i>cxcr4b</i> cloning	subcloning riboprobe in PCS2+ vector	F	5'-GCGCGAATTCGCGAGACCTCTGTTTGTG-3'
	[restriction sites in bold]	R	5'-GCGCCTCGAGGCGAGTGAAATATGCCAGCG-3'
<i>col9a2</i> cloning	subcloning riboprobe in PCS2+ vector	F	5'-GCGCGAATTCCTTTCAGTGTCCAACCAACTG-3'
	[restriction sites in bold]	R	5'-GCGCCTCGAGGATCCTTGCATTCCCATC-3'
<i>col12a1</i> cloning	subcloning riboprobe in PCS2+ vector	F	5'-GCGCGAATTCCTGTATGCTGATGGAGAGG-3'
	[restriction sites in bold]	R	5'-GCGCCTCGAGGCATCATACTGAGCGTAAACC-3'
Cre coding sequence	genotyping for the presence of Cre	F	5'-CGAACGCACTGATTCGACC-3'
		R	5'-AACCAGCGTTTTCGTCTGC-3'
Cre coding sequence (alternative)	genotyping for the presence of Cre	F	5'-GTTTCACTGGTTATGCGGCG-3'
		R	5'-GGTGCTAACCAGCGTTTTTCG-3'
LacZ coding sequence	genotyping for the presence of LacZ	F	5'-GGCGGCTTCGTCTGGGACTG-3'
		R	5'-CAGGCGGCAGTAAGCGGTC-3'
18S shRNA	qPCR quantification of 18S expression	F	5'-AGGAATCCAGTAAGTGGC-3'
		R	5'-GCCTCACTAAACCATCAA-3'
pkd1 shRNA	qPCR quantification of PKD1 expression	F	5'-CTTCCGGTGGACCATCAACG-3'